Water Sorption on Coal: Effects of Oxygen Containing Function Groups and Pore Structure

Ang Liu
Penn State: The Pennsylvania State University
Shimin Liu (szl3@psu.edu)
Department of Energy and Mineral Engineering, G3 Center and Energy Institute, The Pennsylvania State University, University Park, PA 16802, USA https://orcid.org/0000-0001-9612-0047
Peng Liu
Chongqing University
Kai Wang
China University of Mining and Technology - Beijing Campus

Research

Keywords: water vapor, isotherm, surface oxidation, pore collapse, isosteric heat of adsorption

Posted Date: December 17th, 2020

DOI: https://doi.org/10.21203/rs.3.rs-127358/v1

Water sorption on coal: effects of oxygen containing function groups and pore structure

Ang Liu[a], Shimin Liu[a]* Peng Liu[b], Kai Wang[c]

[a]*Department of Energy and Mineral Engineering, G[3] Center and Energy Institute, The Pennsylvania State University, University Park, PA 16802, USA*

[b]*State Key Laboratory of Coal Mine Disaster Dynamics and Control, Chongqing University, Chongqing, 400030, China*

[c]*School of Emergency Management and Safety Engineering, China University of Mining and Technology (Beijing), Beijing 100083, China*

Abstract: Coal-water interactions has profound influences on gas extraction from coal and coal utilization. Experimental measurements on three coals using X-ray photoelectron spectroscopy (XPS), low-temperature nitrogen adsorption and dynamic water vapor sorption (DVS) were conducted. A mechanism-based isotherm model was proposed to estimate the water vapor uptake at various relative humidities, which was well validated with the DVS results. The validated isotherm model of sorption is further used to derive the isosteric heat of water vapor sorption. The pore specific surface area of coal is not the determining parameter that controls water vapor sorption at least during the primary adsorption stage. Oxygen containing degree dominates the primary adsorption, and togethering with the cumulative pore volume determine the secondary adsorption. Higher temperature has limited effects on primary adsorption process. The isosteric heat of water adsorption decreases as water vapor uptake increases, which was found to be close to the latent heat of bulk water condensation at higher relative humidity. The results confirmed that the primary adsorption is controlled by the stronger bonding energy while the interaction energy between water molecules during secondary adsorption stage is relatively weak. However, the thermodynamics of coal-water interactions are complicated since internal bonding interactions within the coal are disrupted at the same time as new bonding interactions take place with the water molecules. Coal has a shrinkage/swelling colloidal structure with moisture loss/gain and it exhibits collapse behavior with some collapses irreversible as a function of relative humidity, which plays a significant role in determining moisture retention.

Keywords: water vapor; isotherm; surface oxidation; pore collapse; isosteric heat of adsorption

1. Introduction

Water is the most common solvent in nature. The properties of water have been extensively investigated in many scientific disciplines such as chemistry, biology, geology[1–4], nanotechnology and materials technology [5]. Water naturally co-exists within coal formation as geological processes apply pressure to dead biotic material over time. Water retention in coal seam can also result from reservoir stimulation using water-based fracturing fluids [6–8]. The resultant water blocking effects because of permanent water-soaking during hydraulic fracturing process exerts a potential risk for reservoir damage and contamination [9]. In addition, water retention in coal has significantly influences on coal utilization including pyrolysis, gasification, liquefaction and combustion [10]. The interactions of coal with retained water is a complex and intricate process compared to gas-coal interactions such as methane, nitrogen, or carbon dioxide[11], which is mainly due to the weak dispersion interaction of water with coal. The complex interactions include hydrogen bonds formation among water molecules, surface chemical species interactions, and the chemisorptive interaction with the coal mineral matter [12]. Unfortunately, the fundamental understandings of water retention behavior, water sorption and transport behaviors, and water-blocking pattern in carbonaceous coal are still largely unknown. The mechanisms of water retention and the associated coal-water interactions lay foundations for coalbed methane (CBM) development and coal utilization.

The water adsorption isotherm on coal has been historically studied in the literature [12–19]. It is generally believed that the combination of weak carbon-water dispersive attractions and strong water-water associative interactions is the controlling factors for the complex behavior of confined water in coal [5]. In other words, the heterogeneity of coal surface (*i.e.* polar oxygen-containing groups *e.g.* carboxyl (-COOH), carbonyl(C=O), and hydroxyl (-OH)) and those active sites usually lead to the primary adsorption through H-bonds formation (Fig.1 (a)) [20,21]. Water molecules are strongly adsorbed on hydrophilic sites provided by oxygen functional groups on the surfaces of coal and mineral matter. This is followed by the secondary adsorption that results in the formation of water clusters and eventually pore filling (Fig.1 (b) and (c)) [5,21].

Despite considerable studies focusing on pertinent coal-water interactions, the water vapor sorption capacity and dynamics of coal are still not well understood due to the complex combinations of coal matrix surface oxidation, pore structure within coal matrices as well as the corresponding thermodynamic changes. In this study, the aim is to investigate the effects of surface oxidation and pore structure on water vapor sorption in coal. We experimentally measured dynamic water vapor sorption for selected coal and we also employed X-rays Photoemission Spectroscopy (XPS) and low-pressure nitrogen adsorption to characterize the oxygen-containing functional groups and pore structure modifications. Based on the mechanism-based understandings on water vapor adsorption on coal, an analytical model is proposed to describe the integrated water vapor sorption isotherms accommodating both the primary adsorption and secondary adsorption. This proposed analytical model was validated against the water vapor sorption isotherms on three coal samples measured at three different temperatures 25℃, 30℃ and 35℃ and relative humidities (R_h) range from 0 up to 0.95. The validated model was used to distinguish the contributions of primary and secondary sorption to the apparent water vapor sorption at different relative humidities. Simultaneously, the isosteric heat of water vapor sorption is modeled and determined by combining the Clausius-Clapeyron equation and the proposed model for quantifying the water vapor sorption isotherm. These results provide a first rational method for analyzing the water sorption behavior and coal-water interactions with potential application of CBM development and coal utilization.

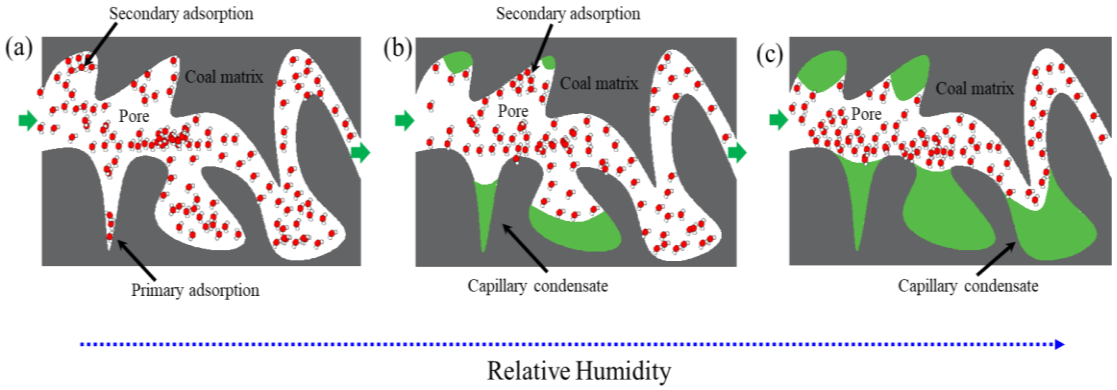

Fig.1: Schematic of water vapor adsorption mechanisms in coal with increasing relative humidity (modified from Sang et al.[22]). (a) Primary adsorption on hydrophilic sites induced by monolayer adsorption

dominates at initial low relative humidity. (b) and (c) Secondary adsorption dominates at higher relative humidity including formation of multilayer adsorption and capillary condensation.

2. Background and previous studies

The oxygen-containing functional groups on the coal surface are believed to determine the water vapor uptake capacity of coal [10,23]. A linear relationship between the water holding capacity and the amount of oxygen functional groups was experimentally observed, proving that the oxygen-containing functional groups are the active sites for water vapor sorption [16]. It has been reported that water vapor primary adsorbs on carboxyl groups through the direct measurement of FT-IR and ionic thermal current [24,25]. It was experimentally observed that the coal rank was an important factor that influences the amount of oxygen functional groups in coal [26]. The large group of experimental data showed that the hydroxyl groups were abundant in brown coal and were predominant with phenolic compounds, followed by the carboxyl groups and methoxy groups (-OCH3). The experimental data also showed that the carbonyl groups can be found in lignite and brown coals but which were in negligible amounts [26]– the results were in line with other investigations [27–29]. Although the oxygen functional groups have slight variations in the trend that follows with rank, the abundance in such functional groups increases towards low rank coals and enhances the hydrophilicity of coal surfaces to increase the water holding capacity [21,29–31].

The presence of oxygen functional groups influences water vapor adsorption mainly at relative-low vapor pressure. The carboxylic groups and hydroxyl groups are the most preferred hydrophilic sites to adsorb water [21]. These preferred oxygen functional groups act as primary adsorption sites for water molecules through hydrogen bonds [19]. Water molecules attached to the primary sites form the secondary adsorption sites on which the water aggregates or clusters can be formed. The clusters accumulate and eventually form into large clusters. The growth of these clusters at the opening of the pores can effectively become a plug to block the entire pore channel [32]. As water vapor pressure increases, the continuous pore filling can essentially occur. The completed isotherm curve of water adsorption is the combined effects of primary and secondary adsorptions. The standard Type II sigmoid shape of water sorption isotherms for bed-moist Yallourn brown coal was reported based on the Brunauer, Deming, Deming and Teller

classification [14]. The sigmoid shape is generally attributed to the combined effects of three separate sorption processes including monolayer sorption, multilayer condensation and capillary condensation [14].

Additionally, the mineral matters and pore size distribution in coals have important influences on water vapor sorption. The majority quantity of mineral matters in coal are clay minerals and quartz [33,34]. It is reported that the dominant mineral quartz in coal generally unreactive even at high temperature, and the interaction between quartz and water can be ignored [21]. Kaolinite, illite, illite/smectite mixed layers and smectite minerals (*i.e.* montmorillonite) are the most abundant clay minerals in coal seams [34,35]. The exchangeable cations that are dissolved in the water are preferred to be attracted if the clay platelets are negatively charged and it will lead to structural layer expansion. Compared to the smectite minerals, the kaolinite clay mineral is vulnerable to swelling and has an immediate swelling effect [36]. The difference in the swelling magnitudes of smectite minerals and other clay minerals mainly attributes to the different swelling mechanisms [37]. As water sorption induced clay mineral swelling can modify the pore structure of coal and its associated mineral clusters. This structural alteration, in turn, is expected to have an important role on the water adsorption of coal. However, the coal swelling with respect to the clay minerals is no less important in the coal material itself, which was confirmed by comparing with the pore volumes of coals (from lignite to anthracite) determined by mercury porosimetry and water uptake capacities, the measurements showed that the adsorbed water contents in coals were about 2~3 times as their pore volumes would indicate [16]. It could be reasonably postulated that the physical change on coal structure of coal-water system as a function of relative humidity plays significant role in determining moisture retention behavior. An important question to be addressed in this paper is how moisture retention capacity and the phenomenon of collapse of coal structure are related.

The above mechanisms behind the physicochemical reactions within coal-water interactions provide the physical understanding of water sorption, pore filling and water condensation, based on which the quantitative evaluation of water uptake amount is essential for engineering application. Many classical sorption-related models are proposed in the past century and the commonly used water adsorption models were summarized below. The classical Langmuir-type adsorption model leads the explanation of the

mechanism of monolayer adsorption is very attractive and often improved [38]. The assumption of monolayer adsorption is widely applied due to the simplicity and giving reliable results, especially for gas adsorption. For water adsorption, the existence of multilayer adsorption exceeds the description range of Langmuir type equation. The Brunauer-Emmett-Teller (BET) model is often used to fit the water vapor adsorption isotherm [39]. The BET multilayer sorption model assumes the secondary adsorption centers exhibit lower binding energies and the thermodynamic properties of the secondary adsorbed water are identical with those of liquid water [18]. But the goodness of fitting results between water vapor uptake and relative humidity based on BET model was found to fail if the relative humidity ranges from 0.35 to higher values. Later, the BET model has been modified and improved by taking two sorption sites into account and better fitting results were arrived [18]. The most classical extension of the BET model is the GAB model [40–42], which is applicable over a more broad range of relative humidities. The difference between the BET and the GAB model is that an additional parameter was introduced into the latter one. The parameter represents the potential of multilayer molecules relative to the potential of bulk liquid [22]. For better modeling of water vapor adsorption, the following specified models are also very popular. The Dubinin-Serpinsky (DS) approach provided a phenomenological model of adsorption of water molecules on primary and the secondary adsorption sites. The DS sorption theory assumes that water molecules firstly adsorb on energy privileged centers (*i.e.* oxygen functional groups) and those adsorbed molecules are capable of providing secondary adsorption centers for water-water interactions through hydrogen bonds [43]. However, one drawback of the DS model is the assumption that the lack of saturation of the secondary adsorption centers [5]. Thus, the original DS model was improved by Dubinin *et al* later and the improved DS equation took the decrease in the number of secondary adsorption centers into account specifically at larger relative pressures. The changes of the secondary adsorption centers with relative pressure increasing will determine the maximal adsorption capacity in the course of water vapor adsorption [44]. To quantify the concentration changes of the secondary adsorption centers, the original DS model was also modified by Barton *et al* [45]. By recalling the DS equation, the primary adsorption capacity on those active oxygen-containing functional groups is incorporated into the integrated mode with one parameter representing the

maximum primary adsorption capacity. To clearly distinguish the contributions of primary and secondary adsorption, the D'Arcy-Watt equation (DW) was proposed by taking the arithmetic summation of the Langmuir-type sorption isotherm and the DS sorption isotherm [46]. Furmaniak *et al*. stated that the main disadvantage of the DW equation is that the simple treatment leads to the implication that all the primary chemisorbed water molecules are not available to act as secondary centers for the formation of water clusters [5]. The DW model was then modified by Furmaniak *et al*. (FG model) by redefining the role of primary adsorption on secondary adsorption [5]. For all above discussed models including DS model, DW model and FG models, no quantitative quantity is involved between those carbon-water dispersive attractions and water-water associative interactions. Malakhov and Volkov proposed the CMMS model (cooperative multimolecular sorption) assumed that per functional group can adsorb one water molecule during primary adsorption stage, followed by the adsorption of two water molecules through hydrogen bonding [5,47]. It was proved that the CMMS theory was applicable to explain water adsorption in carbon-water systems. Specifically, the CMMS theory was found to work well for the interpretation of water vapor sorption isotherms in shapes of I, II, III and V based on IUPAC classification [5,48]. Another classical model related to water adsorption was established by Do and Do (Do-Do model) [49]. It has been postulated that the water adsorption involves a two-step process. The first step is that water molecules are strongly bonded to the primary adsorption sites and conglomerates of water molecules are formed *via* hydrogen bonds. Upon the total number of the adsorbed water molecules constituting the conglomerate reaches five, the conglomerate can tear away from the clusters and has enough dispersive energy to enter the micropores and pore filling starts [5]. In addition, there were also many other semi-empirical and theoretical models proposed and improved in recent years, which were comprehensively summarized in two review publications [5,50].

In terms of thermodynamic theory, it was considered that water vapor adsorption is an exothermic process [18]. The Clausius-Clapeyron equation theoretically defines the isosteric enthalpy of adsorption and generally the isosteric heat of adsorption depends on the surface chemistry and the pore structure. The isosteric heat of water adsorption was reported to have values very close to the latent heat of bulk water

condensation - 45 kJ mol^{-1} at a surface coverage up to 10%. The calculation of the isosteric heat of water vapor sorption was found that the released heat of adsorption at very low relative pressure is equal to the heat of condensation if the pores are too small to accommodate the functional [12]. Busch *et al.* concluded that the isosteric heat of sorption is higher than the heat of condensation when functional groups are present and it was suggested that carbon-water interaction was weak if the isosteric enthalpy of adsorption was low at high surface coverage [12]. The first isosteric enthalpy of adsorption corresponding to the modified DS equation was derived by Kraehenbuehl *et al*. based on the Clausius-Clapeyron equation [51]. In 1958, Darcey reported that the heat of adsorption on Saran charcoals was 63 kJ mol^{-1} for a surface coverage of only 1%, whereas the heat of adsorption approaches the heat of water condensation of 45 kJ mol^{-1} at about 5% surface coverage [52,53]. The Clausius-Clapeyron equation assumes the isosteric heat of sorption is independent of temperature. The net isosteric heat of sorption can be derived based on the Clausius-Clapeyron equation and the total differentiation of adsorption isotherm with respect to temperature at a constant moisture content - the net isosteric heat of sorption is the difference between the isosteric heat and pure water vaporization energy [5,18,19,54]. Additionally, the temperature-dependent and water vapor uptake dependence model of isosteric heat was proposed based on the Dent's multilayer adsorption model [9]. Based on this model, it was found that the ideal gas law would result in an overestimation of the isosteric heat of adsorption at high vapor pressure conditions.

In this study, a mechanism-based isothermal sorption model was proposed to accommodate water vapor sorption on coal considering both primary and secondary adsorptions. The validated isotherm model of sorption was further used to derive the isosteric heat of water vapor sorption. This thermodynamic modeling analyses lay the foundation for elucidating the process of coal-water interaction. These results provide a first rational method for analyzing the water sorption behavior and coal-water interactions.

3. Material and methods

To quantitatively evaluate the coal and water interactions, the surface chemistry and the pore structure of coal were measured experimentally. The surface chemical properties were characterized using X-ray photoelectron spectroscopy (XPS). The pore structures of all the samples were characterized by low-

pressure liquid nitrogen adsorption technique. The water vapor sorption isotherms on three coal samples measured at three elevated temperatures 25℃, 30℃ and 35℃ and relative humidities range from 0 up to 0.95.

3.1. Sample collection and preparation

Two bituminous coal samples from Illinois basin and one bituminous from central Appalachian basin. Two Illinois coals were collected from Herrin seam and Springfield seam and the central Appalachian basin seam was taken from Pocahontas seam. For denotation purpose, we termed Springfield coal as IL-C#1(sub-bituminous coal), Herrin coal as IL-C#2 (sub-bituminous coal) and the central Appalachian basin coal as AB-C (low volatile bituminous coal). All coal samples were collected from the active coal mines. Prior to starting the actual tests, the prepared samples were kept in an environmental chamber under controlled conditions of temperature and humidity equilibration.

3.2. XPS measurements

XPS is a quantitative and reliable technique using X-rays to remove electrons from the C1s and O1s levels of coal sample [55]. The energies of the emitted electrons depend on the atoms present and thus the chemical composition of the material. This allows the quantification of elemental composition in the parts-per-thousand range, as well as the nature of the chemical bonds. XPS can thus provide a measure of surface oxidation degree through the O/C ratio, quantify the different types of carbon functionalities present on the coal, indicate the formation of chemical bonds, and evaluate the physisorption of molecules [56,57]. XPS experiments were performed using a Physical Electronics VersaProbe II instrument equipped with a monochromatic Al kα x-ray source (hν = 1486.7 eV) and a concentric hemispherical analyzer. Charge neutralization was performed using both low energy electrons (<5 eV) and argon ions. The binding energy axis was calibrated using sputter cleaned Cu (Cu $2p_{3/2}$ = 932.62 eV, Cu $3p_{3/2}$ = 75.1 eV) and Au foils (Au $4f_{7/2}$ = 83.96 eV). Peaks were charge referenced to CHx band in the carbon 1s spectra at 284.5 eV [58]. Measurements were made at a takeoff angle of 45° with respect to the sample surface plane. This resulted in a typical sampling depth of 3-6 nm (95% of the signal originated from this depth or shallower).

Quantification was done using instrumental relative sensitivity factors (RSFs) that account for the X-ray cross section and inelastic mean free path of the electrons. Data analysis and fitting were performed with CasaXPS software authorized in MCL at The Pennsylvania State University.

3.3. Low-pressure liquid nitrogen adsorption

The low-temperature nitrogen adsorption (LTNA) test at 77K was performed on three coal samples (60-80mesh) using a Micrometrics TriStar II 3020 Version 2.0 using the static volumetric method. Prior to the test, the prepared coal samples were degassed under vacuum for approximately 12h. The isotherms of nitrogen adsorption were obtained under a wide range of relative pressures (p/p_0) from 0.01 to 0.99, where p is the equilibrium pressure and p_0 is the saturation pressure. The pore properties including the specified surface area (SSA), pore volumes (PV) and pore size distribution (PSD) were defined by combining the standard Brunauer-Emmett-Teller (BET) model and density functional theory [59,60].

3.4. Dynamic water vapor sorption

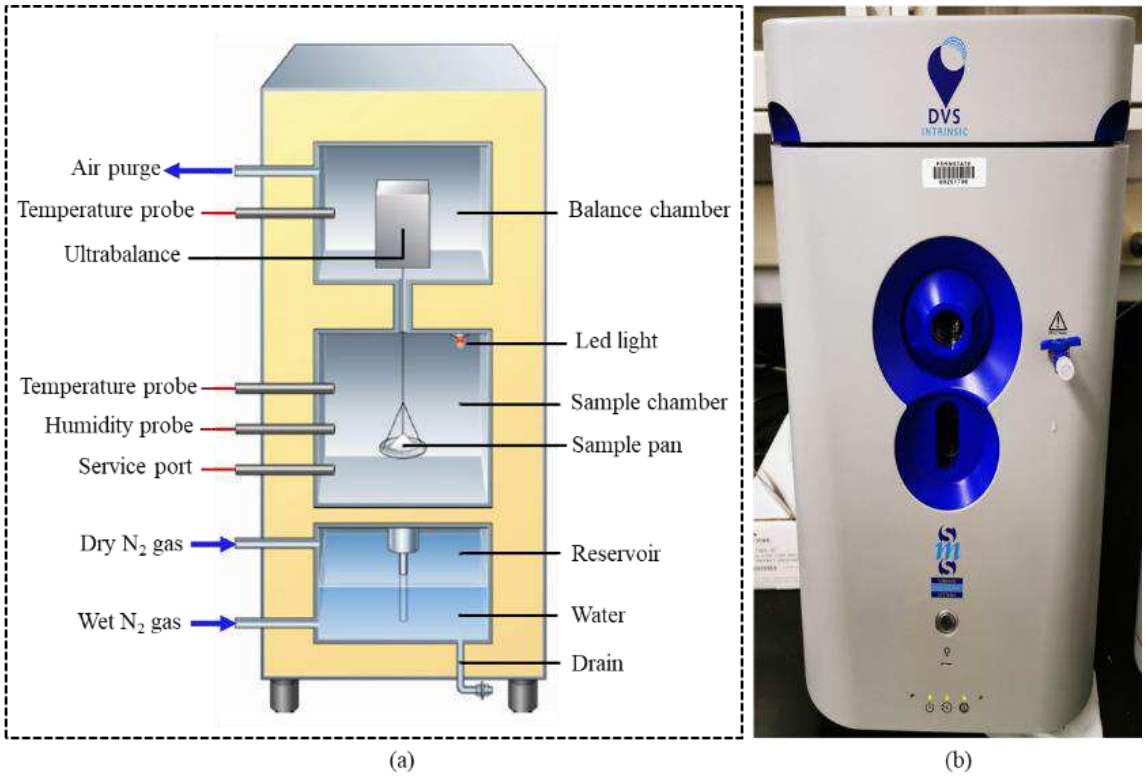

Fig.2: Schematic and lab-view of the DVS instrument

The Dynamic Vapor Sorption (DVS) Intrinsic is designed to accurately measure the mass changes of sample as it sorbs precisely controlled concentrations of water vapors in a gas (*i.e.* nitrogen) carrier gas. The instrument used in this study is equipped at our lab as shown in Fig.2. The mechanism behind the DVS instrument is a gravimetric method-based ultra-sensitive recording microbalance. The ultra-sensitive recording microbalance is capable of measuring changes in sample mass with the accuracy of one ppm. As the air with a known relative humidity passes over the sample, the changes in the mass sample are continuously recorded. In Fig.2, the DVS instrument contains three main parts including the reservoir chamber, sample chamber and the balance chamber. Relative humidity is the ratio of the partial vapor pressure to the saturation vapor pressure of water at a given temperature. Each required and tested relative humidity is generated by accurately mixing dry (dry N_2 stream) and saturated vapor gas flows (wetting N_2 stream containing 100% humidity) in the proportional mixture, using precision mass flow controllers. The relative humidity sensor and temperature probe located near the sample (sample chamber) are used to verify system performance. In the sample chamber, the sample is loaded on sample pan under the given temperature. The gas flow with required relative humidity from the reservoir chamber passes over the sample and the changes in the sample mass occur as time increases due to water uptake. The changes in sample mass are continuously monitored and recorded by the data acquisition system. It should be noted that there is an additional temperature probe and an air purge in the balance chamber. To ensure the accurate performance of the ultra-sensitive recording microbalance apart from the potential condensation of water vapor in the balance chamber, the dry purge gas with a fixed flow rate of 70 sccm and a temperature of 40 ℃ is continuously flowed.

In this study, the isotherms of water vapor sorption on coals are targeted to be obtained under various relative humidities and temperatures. The operation programs for three full circles under three different temperatures 25℃, 30℃ and 35℃. The water vapor adsorption and desorption processes were run in the relative humidity range from 0 to 0.95 and then back to 0 after one complete cycle. In Fig.3, the raw data recovered from the dynamic vapor sorption analyzer for IL-C#1was plotted. Under initial dry condition ($R_h \sim 0\%$), any residual water can be removed until a constant value which is the sample mass

[22]. Each coal sample was placed on the sample pan for the tests. The equilibrium state under different relative humidities is defined when mass change is less than or equal to 0.002% per minute and maintained stable for ten minutes. The average of the last three points was taken as the final equilibrium value. Water vapor adsorption/desorption isotherms are then directly estimated and computed from the difference between the reference mass and the equilibrium mass at any given prescribed relative humidity.

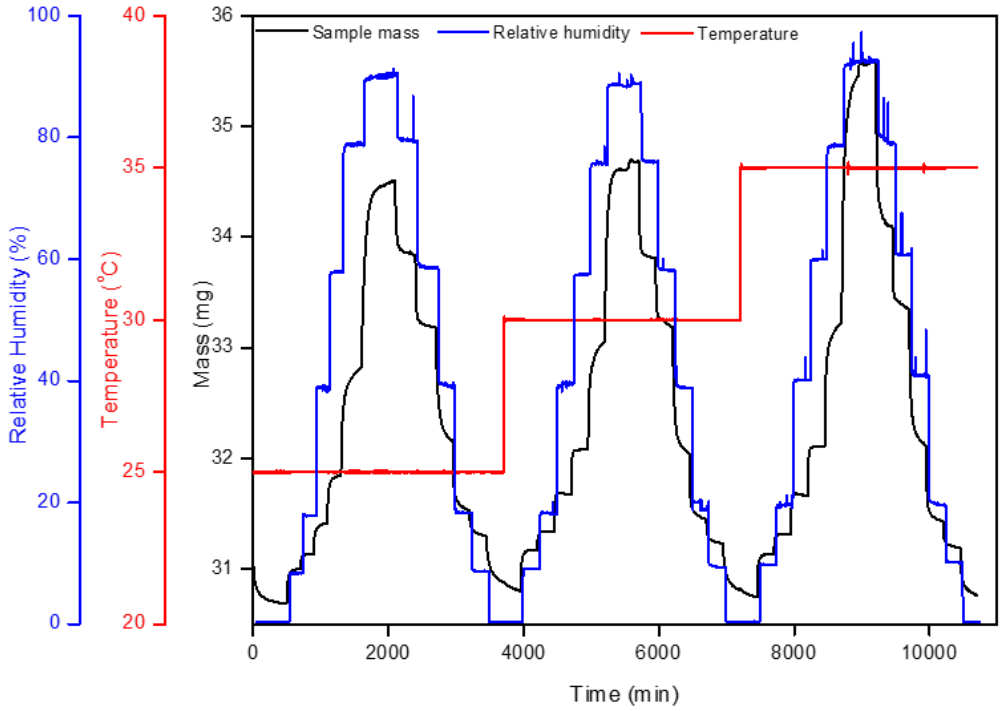

Fig.3: Three full circles of water vapor sorption measurements - raw data from DVS instrument dynamic vapor sorption analyzer for IL-C#1

4. Water vapor sorption modeling

The aim of this study was to investigate the process of water vapor sorption on coal. Although principally those hydrophobic adsorbents may contain significant numbers of adsorption sites that can interact with water molecules, it is generally believed that the combination of carbonaceous surface-water dispersive attractions and water-water associative interactions are responsible for the complex behavior of water vapor confined in carbonaceous pores [5]. A mechanism-based isotherm model for water vapor sorption on coal was proposed which can explicitly accommodate both primary and secondary adsorption.

Based on the isotherm model of water vapor sorption, the approach for calculating the isosteric heat of water vapor sorption was then provided by combing the Clausius-Clapeyron equation.

4.1. Water vapor sorption isotherms

Previous studies showed that the difference in the shape of water vapor sorption isotherms is caused by the combined effects of primary and secondary adsorptions [12,16,17,29,61]. Water vapor is presumed to be firstly and directly adsorbed on the primary sorption sites in the presence of hydrophilic functional groups due to their strong binding energy with water molecules. Subsequently, those adsorbed water molecules occupied on primary sites are considered as the secondary centers for the formation of water aggregates or clusters. For the simplification of modeling water vapor isotherm, it is assumed that the secondary adsorption starts only after the monomolecular coverage is achieved during the primary adsorption stage.

The Langmuir model, leading to the explanation of the mechanism of adsorbate sorption behavior [38]. For the application of Langmuir-type model, the surface of adsorbent is assumed as homogeneous and there is a maximum surface concentration of adsorbate adsorbed on adsorbent in monolayer pattern. An additional assumption is that adsorption sites are identical and mutually independent, and each site can accommodate only one molecule. Thus, the Langmuir-type model is appropriate to describe the process of the monomolecular coverage with the increase in water vapor pressure, the Langmuir-type sorption model for water vapor sorption at specified relative humidity can be introduced and expressed as [5,38]:

$$m_{pri} = \frac{m_L R_h}{R_L + R_h} \tag{1}$$

where, m_{pri} is the primary adsorption of water vapor at specified relative humidity, mmol/g; m_L is the maximum water vapor uptake corresponding to a complete monolayer coverage, mmol/g; R_L is the relative humidity at which the measured adsorption content is equal to ½ m_L, dimensionless.

For the secondary adsorption, the phenomenological Dubinin-Serpinsky approach was introduced in the mid-1950s to accommodate the formation of water aggregates or clusters on energy privileged sites

acting as primary adsorption centers for water on predominantly hydrophobic carbon surface. The original Dubinin-Serpinsky model can be written as[43]:

$$m_{sec} = \frac{m_0 ckR_h}{1-ckR_h} \quad (2)$$

where, m_{sec} is the secondary adsorption of water vapor at specified relative humidity, mmol/g; m_0 is the surface concentration of the energy privileged hydrophilic adsorption centres, mmol/g; c is the ratio between the rate constants of adsorption and desorption, dimensionless; k represents the loss of the secondary sites in the course of adsorption, dimensionless, which is a constant whose magnitude is fixed by the condition that for $R_h = 1$. In the original Dubinin-Serpinsky approach, k is treated as a part of c and is equal to unity [5]. It should be noted that the parameter is also regarded as unity in this study.

Ideally, all the primary adsorbed water molecules can become the secondary adsorption centers and are available for multilayer formation of water aggregates or clusters. In other words, the water vapor uptake of the energy privileged hydrophilic adsorption centers (m_0) in Eq. (2) can be regarded as the primary adsorption of water vapor calculated from Langmuir-type adsorption model (m_{pri}) (Eq. (1)). However, previous studies showed that not all the water molecules can be considered as the secondary adsorption centers for the formation of water clusters mainly due to the mechanical constraints to pore structure, swelling or steric effects [62]. Therefore, the parameter "ω" was introduced to accommodate the non-perfectly multilayer formation building from the monomolecular coverage [5]– the water vapor uptake of the energy privileged hydrophilic adsorption centers (m_0) can be calculated from $m_0 = \omega m_{pri}$, where $0 \leq \omega \leq 1$. Totally, the isothermal curve of water vapor sorption over the entire range of relative humidity is summation of the primary adsorption and secondary adsorption and mathematically it can be expressed as:

$$m = m_{pri} + m_{sec} = \frac{m_L R_h (1-cR_h+c\omega R_h)}{(R_L+R_h)(1-cR_h)} \quad (3)$$

where, ω is the ratio of the amount of primary adsorption centers involved in the formation of the secondary adsorption centers, dimensionless. It can be seen that if all the adsorbed molecules on primary centers can be treated as the secondary centers ($\omega = 1$), Eq. (3) can be reduced to the generalized D'Arcy-Watt model [5] – it should be noted that the generalized D'Arcy-Watt model is equivalent with the GAB model. The

GAB model is an extension of the classical BET model if the constant c is taken as unity. Based on the water adsorption isotherm measured on oxidized nanoporous carbon, Barton *et al.* found that only 17% of the primary sites can be performing as the secondary centers[62]. However, others suggested that those water molecules adsorbed at the primary sites can form up bonds for the formation of microclusters consisting of two to three molecules[63,64]. Furmaniak et al. summarized that the values of ω can be lower than unity or can be close to three for carbonaceous materials[5]. In this study, ω is regarded as unity. Thus, we proposed the model by assuming all the adsorbed water molecules through primary adsorption can provide new sorption centers for the formation of water clusters.

4.2. Isosteric heat of water vapor adsorption

The adsorption heat of water vapor indicates that adsorption is a strong function of surface chemistry. If the isosteric heat of water vapor adsorption is assumed as independence of temperature, the Clausius-Clapeyron equation defines the isosteric heat of adsorption as:

$$\frac{\Delta H}{RT^2} = \left[\frac{\partial \ln(p)}{\partial T}\right]_m \tag{4}$$

where, ΔH is the isosteric enthalpy of water vapor adsorption at a specific water content (mmol/g) - the subscript m represents the given water content, kJ·mol^{-1}; p is the equilibrium water vapor pressure, kPa; R is the universal gas constant, J·mol^{-1}·K^{-1}; T is the temperature, K.

The water adsorption isotherm, Eq. (3), written in the form with respect to water vapor pressure, can be expressed as:

$$m = \frac{m_L p(p_0 - cp + c\omega p)}{(p_0 R_L + p)(p_0 - cp)} \tag{5}$$

where, $p_0$is the saturated pressure of water vapor at given temperature, kPa.

Taking the logarithm on both sides of Eq. (5) and then taking the total differentiation of which with respect to temperature at a constant moisture content gives:

$$0 = \frac{\partial \ln(\frac{m_L p}{p_0 R_L + p})}{\partial T} + \frac{\partial \ln(\frac{p_0 - cp + c\omega p}{p_0 - cp})}{\partial T} \tag{6}$$

Simplifying and then rearranging the terms gives:

$$\frac{dlnp}{dT} = \frac{\frac{p_0 R_L}{p_0 R_L + p}\frac{dlnR_L}{dT} + \left[\frac{R_L}{p_0 R_L + p} + \frac{c\omega p}{(p_0 - cp + c\omega p)(p_0 - cp)}\right]\frac{dp_0}{dT} - \frac{p\omega p_0 c}{(p_0 - cp + c\omega p)(p_0 - cp)}\frac{dlnc}{dT} - \frac{d\ln m_L}{dT}}{\left[\frac{p_0 R_L}{p_0 R_L + p} + \frac{c\omega p p_0}{(p_0 - cp + c\omega p)(p_0 - cp)}\right]} \quad (7)$$

In Eq. (7), the saturated water vapor pressure (p_0) is a temperature-dependent parameter. The August–Roche–Magnus formula provides a very good approximation to calculate the saturated water vapor pressure [65]:

$$p_0 = 0.61094 \exp\left(\frac{17.625T - 4814.269}{T - 30.11}\right) \quad (8)$$

where, p_0 is the saturated water vapor pressure, kPa; T is temperature, K.

Mathematical modeling and the analysis of experimental data show that the temperature-dependent parameter c plays an important role in the description of the shape of the water adsorption isotherm. Kraehenbuehl and co-workers were the first to have derived the relationship between immersion calorimetry and the temperature-dependent parameter c, can be expressed as [51]:

$$c = c_0 \exp(q_0/RT) \quad (9)$$

where, c_0 is the experimental fitting parameter, dimensionless; q_0 is enthalpy of immersion into water, kJ·mol^{-1}.

Additionally, mathematical modeling and the analysis of experimental data show that the temperature-dependent parameter R_L plays an important role in the description of the shape of the water adsorption isotherm:

$$R_L = R_{L0} \exp(q_L/RT) \quad (10)$$

where, q_L is the adsorption energy on primary sites, kJ·mol^{-1}; R_{L0} is the experimental fitting parameter, dimensionless.

By taking the differentiations of Eqs. (8) and (9) with respect to temperature, and then introducing them into Eq. (7), yields:

$$\frac{dlnp}{dT} = \frac{\frac{p_0 R_L}{p_0 R_L + p}\frac{dlnR_L}{dT} + \left[\frac{R_L p_0}{p_0 R_L + p} + \frac{c\omega p p_0}{(p_0 - cp + c\omega p)(p_0 - cp)}\right]\frac{4283.58}{(T - 30.11)^2} - \frac{p\omega p_0 c q_0}{(p_0 - cp + c\omega p)(p_0 - cp)RT^2} - \frac{d\ln m_L}{dT}}{\left[\frac{p_0 R_L}{p_0 R_L + p} + \frac{c\omega p p_0}{(p_0 - cp + c\omega p)(p_0 - cp)}\right]} \quad (11)$$

By introducing Eq. (11) into Eq. (4), and then inserting Eqs. (8), (9) and (10) into Eq. (11), finally yields:

$$\Delta H = \frac{\frac{p_0 R_L q_L}{p_0 R_L + p} + \left[\frac{R_L p_0}{p_0 R_L + p} + \frac{c\omega p p_0}{(p_0 - cp + c\omega p)(p_0 - cp)}\right] \frac{4283.58RT^2}{(T-30.11)^2} + \frac{p\omega p_0 c q_0}{(p_0 - cp + c\omega p)(p_0 - cp)} - \frac{d \ln m_L}{dT}}{\left[\frac{p_0 R_L}{p_0 R_L + p} + \frac{c\omega p p_0}{(p_0 - cp + c\omega p)(p_0 - cp)}\right]} \quad (12)$$

Eq. (12) gives the expression for calculating the isosteric heat of water vapor adsorption. Previous studies shown that the term $\frac{d \ln m_L}{dT}$ is very small and which can be ignored [54].

By ignoring the term '$\frac{d \ln m_L}{dT}$' on the right side of Eq. (12), the simplified model for calculating the isosteric heat of water vapor adsorption can be expressed as:

$$\Delta H = \frac{\frac{p_0 R_L q_L}{p_0 R_L + p} + \left[\frac{R_L p_0}{p_0 R_L + p} + \frac{c\omega p p_0}{(p_0 - cp + c\omega p)(p_0 - cp)}\right] \frac{4283.58RT^2}{(T-30.11)^2} + \frac{p\omega p_0 c q_0}{(p_0 - cp + c\omega p)(p_0 - cp)}}{\left[\frac{p_0 R_L}{p_0 R_L + p} + \frac{c\omega p p_0}{(p_0 - cp + c\omega p)(p_0 - cp)}\right]} \quad (13)$$

5. Results and discussions

5.1. Experimental results

5.1.1 O/C values

To evaluate the surface hydrophilicity of coal matrix of three coal samples, we used the atom ratios of oxygen to carbon (O/C) determined by XPS to represent the degrees of surface oxidation as suggested by previous studies [55–57]. Strictly, 'oxygen atom' in this sense means that the oxygen atoms embed into the oxygen-containing functional groups such as -OH, -COOH, C=O, C-O-C, and others. The XPS results were summarized in Tab.1. Based on the XPS results, both the two Illinois coal samples contained C, O, N and S as well as various mineral-related elements including Al, Si and Fe, while the central Appalachian coal sample only contained C, O, and S elements. The contents of carbon element in samples IL-C#1 and IL-C#2 show slight difference - as ~71.6% and ~ 70.2%, respectively, while the sample AB-C has extremely high content of carbon element, up to ~ 96%. The differences in the carbon contents between the sub-bituminous samples (IL-C#1 and IL-C#2) and low volatile bituminous coal sample (AB-C) are expected due to the degree of coalification. As differentiating by coal ranks from lignite, to subbituminous, then to

bituminous, and finally to anthracite, the coalification process can change the buried plant matter to an ever denser, drier, more carbon rich coal macerals. There has no N element was detected in AB-C sample while IL-C#1 and IL-C#2 have ~ 1.9 % and 1.6%, respectively. Further, sulfur was present in IL-C#1 and IL-C#2 as a mixture of R-S and sulfate. The oxygen contents in IL-C#1 and IL-C#2 are ~20.7% and 22.9% respectively, while in AB-C it only contained 3.8% oxygen elements. It should be noted that contents of oxygen elements in all coal samples do not solely attributed from the presence of oxygen-containing functional groups. As shown in Tab.1, oxygen elements present in inorganic matters such as $SO4^{2-}$, SiO_2 should not be counted. By subtracting the oxygen atoms contained in inorganic matters, the values of O/C ratio representing the surface oxidation degrees were shown Tab.1. The results shown IL-C#2 has the highest oxygen containing degree (0.18) among these samples, followed by IL-C#1(0.13), which is about 4.5 times than AB-C does (0.04).

Tab.1: Concentration of elements detected (in atom %)

Sample	C	N	O	Si†	SO_4^{2-}	R-S	S^{total}	O/C*
IL-C#1	71.6	1.9	20.7	1.8	1.5	2.5	4.0	0.13
IL-C#2	70.2	1.6	22.9	2.6	0.9	1.8	2.7	0.18
AB-C	96.0	-	3.8	-	-	-	0.2	0.04

Note: † Samples also contained ~1% Al and ~0.5% Fe. O/C value of IL-C#1=(20.7-4*1.5(SO_4^{2-})-2*1.8(Si)-1.5(Al &Fe))/71.6; O/C value of IL-C#2=(22.9-4*0.9(SO_4^{2-})-2*2.6(Si)-1.5(Al &Fe))/70.2; O/C value of AB-C=3.8/96.

5.1.2 Pore size distribution and pore volume for three tested coals

Based on the low temperature nitrogen adsorption results, the nitrogen adsorption isotherms for the tested coal samples were shown in Fig. 4. A distinctive difference in their nitrogen sorption capacities mainly results from their different physicochemical properties such as the surface chemistry property, surface area, pore size distribution, and pore volume *et al*. According to the IUPAC classification, all the

three samples exhibit an H3-type hysteresis loop suggesting the process of capillary condensation and evaporation within the mesopores, which also suggests the contained slit-shape pores in coals [60].

Based on the nitrogen adsorption data, BET model and the density functional theory, the PSD, specified surface area (SSA) quantified by BET model and the cumulative pore volume were plotted in Fig.5 (a) and (b). In Fig.5 (a), the PSDs were plotted. Mesopores in the range 1 nm to 100 nm are well developed in IL-C#1. The IL-C#2 and AB-C samples have the similar PSDs. In Fig.5 (b), the cumulative pore volumes for the three samples were measured to be 0.0137 cm^3/g, 0.0014 cm^3/g and 0.002 cm^3/g. IL-C#1 has the largest cumulative pore volume for pore sizes in the range 1nm to 100 nm, which is about 6.85 times than AB-C sample does. Results of BET SSA show that IL-C#1 has the highest SSA (8.032 m^2/g), followed by IL-C#2 (0.490m^2/g) and central Appalachian coal sample (1.120 m^2/g). The effects of the cumulative pore volumes and BET SSA on water vapor adsorption are compared and discussed in Section 5.2.1.

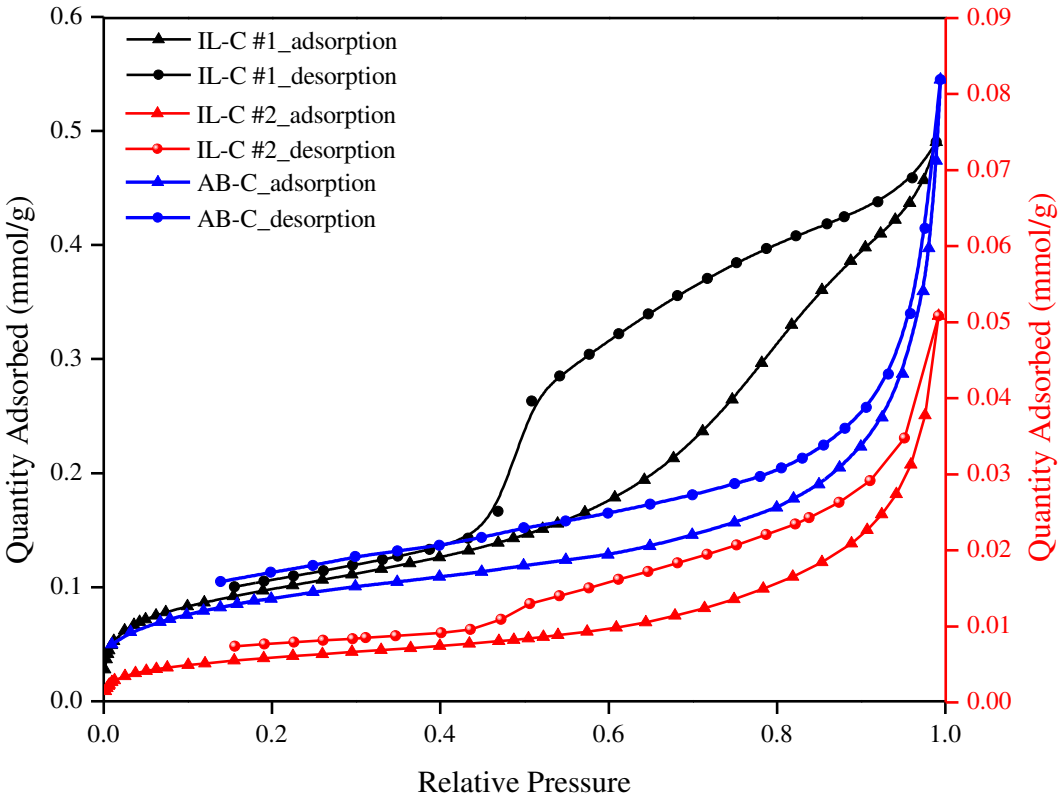

Fig.4: Low-temperature nitrogen adsorption isotherms

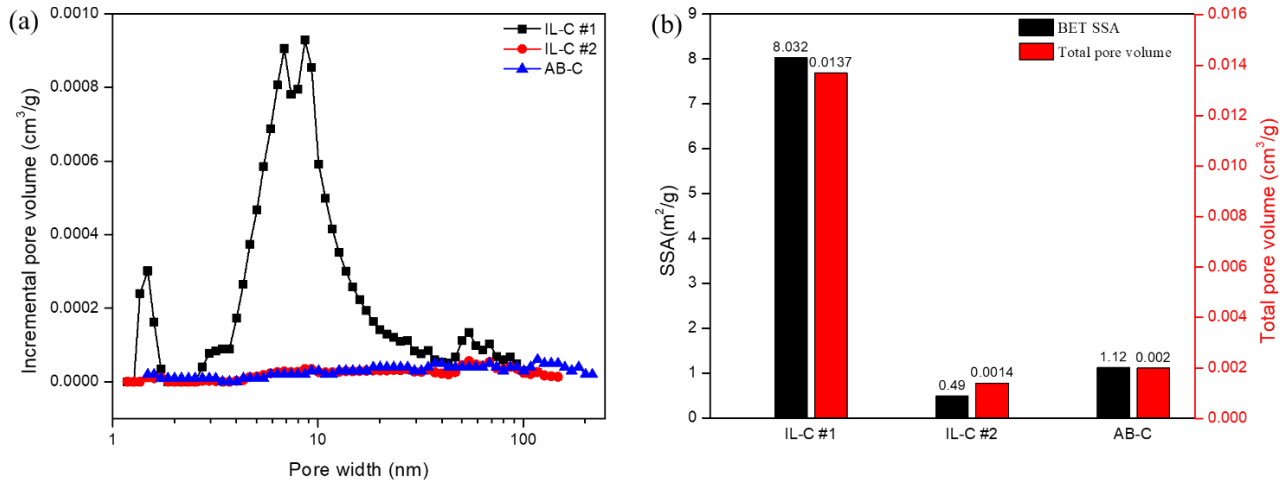

Fig.5: Pore properties based on BET model and density functional theory. (a) Pore size distribution and (b) BET SSA and cumulative pore volume

5.1.3 Dynamic vapor sorption isotherms

The ad/desorption isotherms for the three coal samples at 25°C, 30°C and 35°C were plotted in Fig. 6. According to the IUPAC classification [48], the type II sorption isotherms were observed on all three coals. In Fig. 6(a1), (b1) and (c1), the amounts of water vapor uptakes continuously increase with the increase in relative humidity at all given temperatures. Under the same temperature, it can be observed that IL-C#1 has the highest water holding capacity, followed by IL-C#2 in the same order of magnitude, while the AB-C sample has the lowest water holding capacity. It can be roughly estimated that the amount of water uptake of AB-C sample is about ten times less than the two Illinois basin samples. As the increase of relative humidity, two bending regions were observed over the entire sorption isotherms. This is shown as the amount of water vapor uptake nonlinearly increases in a convex shape at relatively low relative humidity, followed by the concave increasing trend at high relative humidity (Fig.6). Interestingly, even the total amounts of water vapor uptakes of IL-C#1 and IL-C#2 show distinctive difference, the presences of the inflection points do not show obvious differences with both occurring at the relative humidity of ~ 0.2. Additionally, the inflection point for AB-C sample also occurs at around relative humidity of ~ 0.2 but the corresponding amount of water vapor uptake at this point is about ten times less than the other two samples. Previous studies shown that the shape of the isotherm is the combination of monolayer adsorption on

primary adsorption sites, followed by the secondary adsorption on sites provided by primary adsorbed water molecules [13,18,66]. Among the possible mechanism-based factors influencing the primary and secondary adsorption processes including mineral components, coal rank, surface chemistry and pore properties et al., the oxygen containing groups and the pore properties were quantified in Section 5.1.1 and 5.1.2. As shown in Tab.1, the results showed that the oxygen containing degrees of IL-C#1 and IL-C#2 show slight difference for O/C ratio with 0.13 and 0.18, respectively. But both IL coals have much higher O/C ratios than that of AB-C sample of value at 0.04. In Section 5.1.2, the results determined from the low temperature nitrogen adsorption shown that IL-C#1 has obviously developed pore network than IL-C#2, while the latter one has similar pore network as AB-C sample. Thus, it is useful to analyze the effects of oxygen containing degree and pore properties on primary and secondary adsorptions.

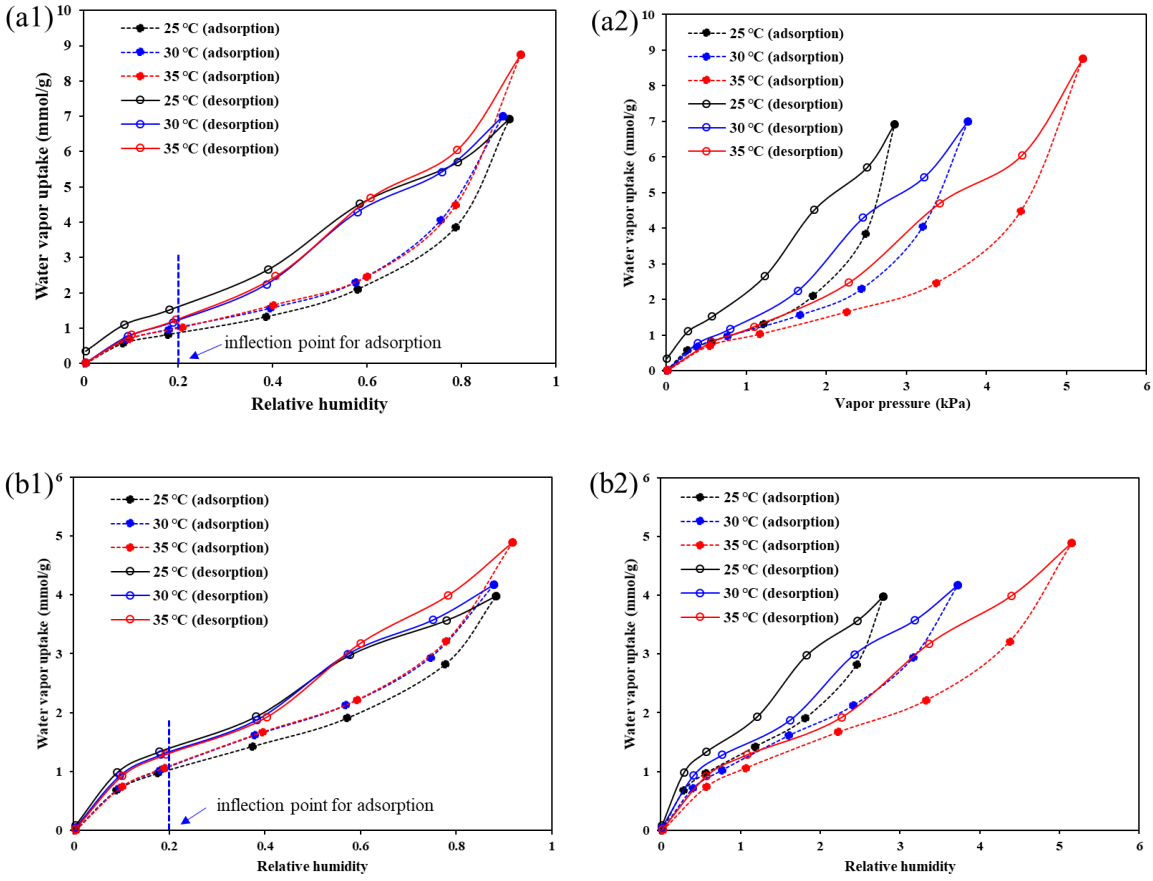

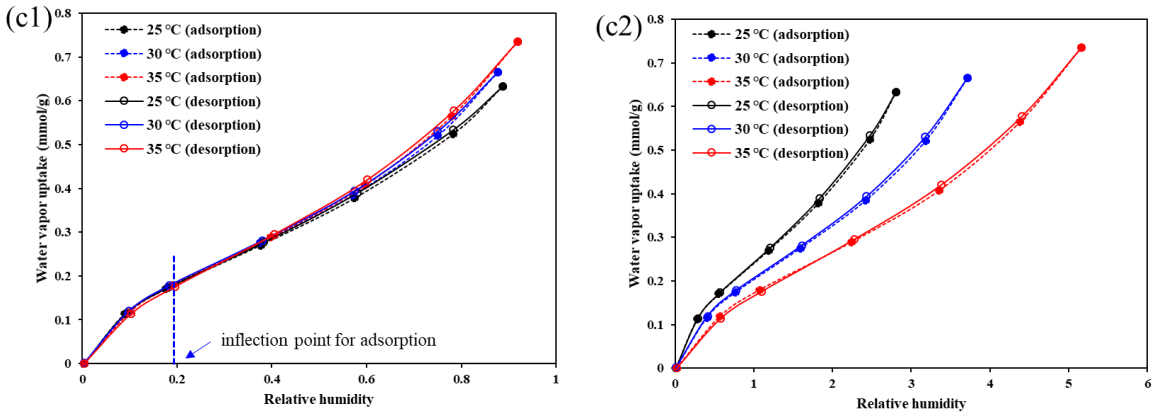

Fig.6: Water ad/desorption isotherms with respect to relative humidity/vapor pressure: (a1) and (a2) IL-C#1 sample; (b1) and (b2) IL-C#2 sample; (c1) and (c2) AB-C sample

The temperature is an important factor impacts water vapor adsorption, but the difference is not obvious by plotting the sorption isotherms with respect to relative humidity (Fig. 6(a1), (b1) and (c1)). The isotherms of water vapor uptake with respect to vapor pressures at different temperatures were plotted in Fig. 6(a2), (b2) and (c3). The temperature has negative effect on the adsorption uptake resulting in a higher adsorption uptake at lower temperature. Theoretically, as the increase of vapor temperature, the movement activities of water molecules are expected to elevated and water molecules should have enough energy to get rid of intermolecular attraction forces between the sorptive sites and water vapor. However, temperature makes only subtle difference to the isotherms at relatively low relative humidity and the difference at higher relative humidity is much apparent as data indicated in Fig. 6. As illustrated in Fig.7, the hydrogen bonds can be formed between the water molecules with the oxygen-containing functional groups mainly during the primary adsorption stage (Fig.7(b)). With relative humidity increasing, the hydrogen bonds can also be formed between the free water vapor molecules and the primary adsorbed water molecules (Fig.7(a) and (b), but the bonding energy is relatively weak by comparing with the energy of hydrogen bonds within the primary adsorption. Thus, the temperature effects can be interpreted as the stronger binding energy between water molecule and coal surface (Type II) than the attraction energy between water molecules (Type I) in Fig.7(a). The higher temperature increases the energy of water molecules, which may overcome the attraction energy between water molecules during secondary adsorption period, but may not overcome the

energy barrier induced by binding energy between water molecule and oxygen-containing functional groups on the surface of coal matrix.

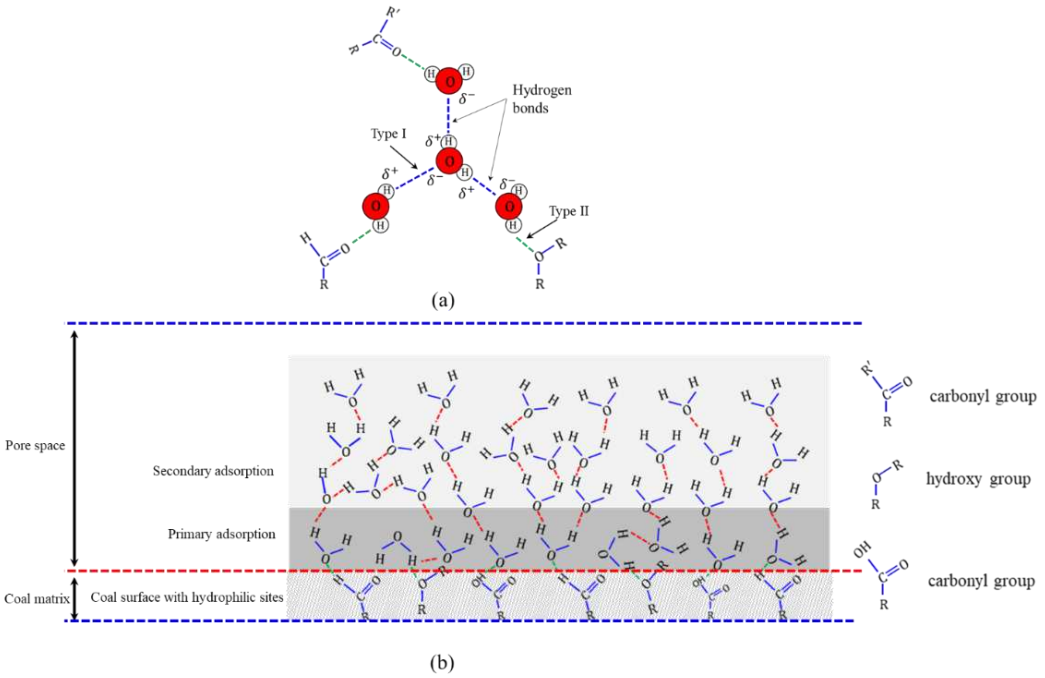

Fig.7: Hydrogen bonds of primary adsorption on coal surface with hydrophilic sites and secondary adsorption formed on primary centers.

5.2. Modeling results and discussions

5.2.1 Adsorption isotherms of considering both primary and secondary adsorption

Based on the experimental results, the isotherm model, combing both primary adsorption (Eq. 1) and secondary adsorption (Eq. 2), was proposed as Eq. 3. The parameters, m_L and R_L, are quantified to evaluate the water vapor uptake induced by the primary adsorption and the parameter c is involved to characterize the secondary adsorption process. Based on Eq. 3, the modeled results agree well against with the experiment data with $R^2 > 0.99$ (Fig.8 (a1), (b1) and (c1)), and the fitting results are listed in Tab. 2. Based on the fitted results of m_L, R_L and c, the contributions of primary and secondary adsorption to the entire adsorption isotherm were calculated and plotted in Fig.8 (a2), (b2) and (c2). In addition, the effects of temperature on primary and secondary adsorptions were evaluated through the changes of corresponding

parameters m_L, R_L and c. Based on the fitting results, the questions raised in last section about the effects of oxygen containing degree and pore properties on primary and secondary adsorption and whether these factors can affect the sorption stages in different order can be mechanistically discussed and revealed.

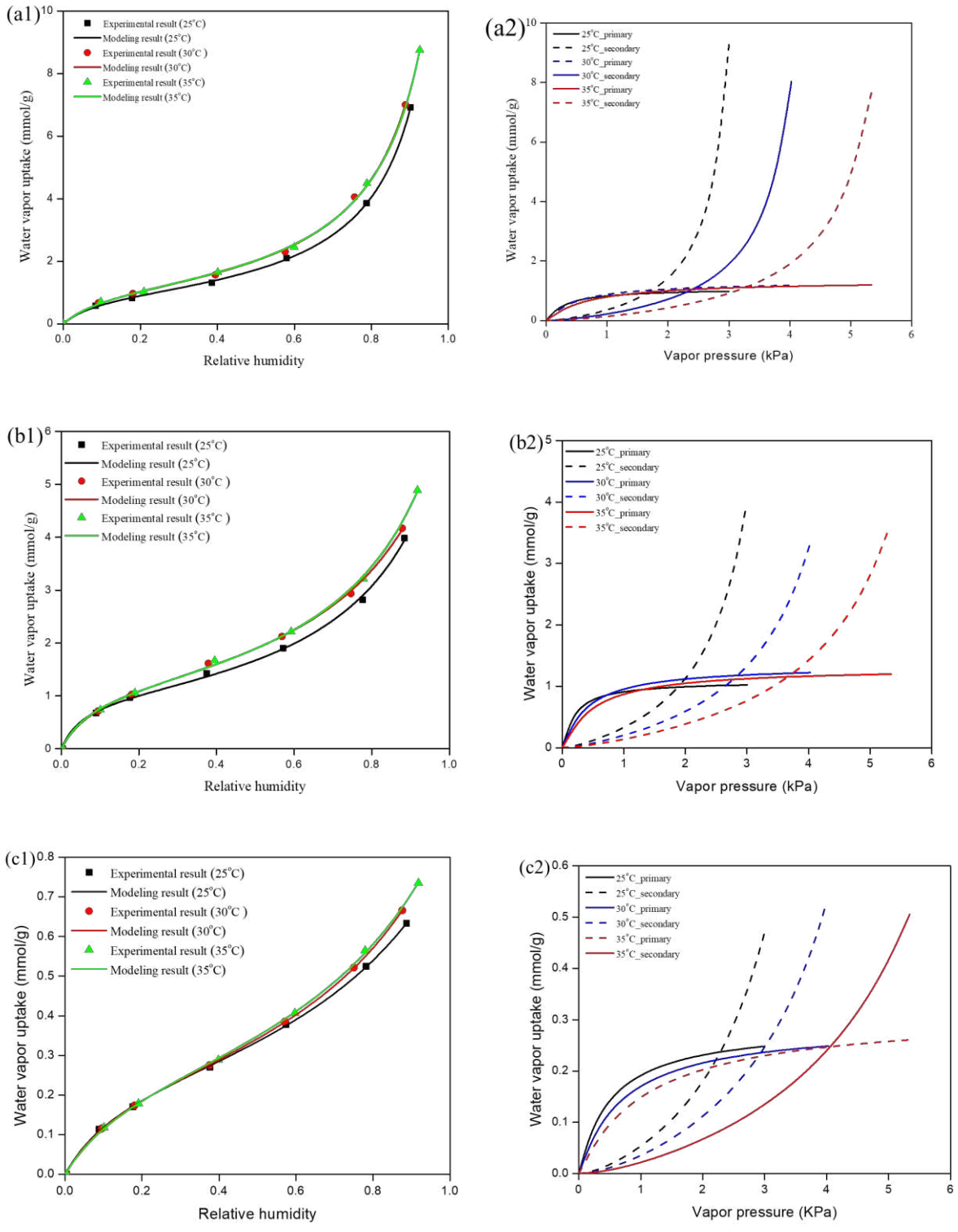

Fig.8: Comparisons between the experiment data and modeling results: (a1) and (a2) IL #1; (b1) and (b2) IL-C#2; (c1) and (c2) AB-C

Tab.2: Modeling results

Sample number	Coal rank	Temperature	Model coefficients			R^2
			m_L	R_L	c	
IL-C#1	Sub-bituminous	25℃	1.086	0.100	0.952	0.99
		30℃	1.330	0.121	0.938	0.99
		35℃	1.348	0.123	0.933	0.99
IL-C#2	Sub-bituminous	25℃	1.090	0.062	0.839	0.99
		30℃	1.347	0.096	0.805	0.99
		35℃	1.350	0.100	0.800	0.99
AB-C	Low volatile bituminous	25℃	0.291	0.164	0.730	0.98
		30℃	0.293	0.169	0.721	0.99
		35℃	0.315	0.197	0.706	0.99

The parameters m_L based on the Langmuir-type primary adsorption representing the maximum water vapor uptake corresponding to a complete monolayer coverage. We first examined the modeling results of the two sub-bituminous coals from Illinois basin. Under the same temperature, taking 25℃ for example, the primary adsorption capacity of IL-C#2 (~1.090 mmol/g) is slightly higher than IL-C#1 (~1.086 mmol/g) (Tab.2), which correlate the results of their oxygen containing degrees representing by O/C values in Tab.1. We also observed that the BET SSA of IL-C#1 (8.032m^2/g) is about 16.39 times than that of IL-C#2 (0.49 m^2/g), as illustrated in Fig.5, but it seems that the surface area cannot determine the water holding capacity of coal surface specifically at primary adsorption stage. Further, the measurement results between IL-C#2 and AB-C show that their BET SSAs have some considerable difference (0.49 m^2/g and 1.12 m^2/g respectively), but the modeling results (at 25℃) showed that the maximum water holding capacity at primary adsorption stage is ~0.291 mmol/g of AB-C, which is ~ 3.75 times less than IL-C#2

does (~1.090 mmol/g). The big difference between these two coal samples can be attributed to the distinction of oxygen containing degrees, with O/C value of IL-C#2 (~0.18) is ~4.49 times than AB-C (~0.040). The observation can also be confirmed by comparing the results between IL-C#1and AB-C showing that IL-C#1bhas approximately 3.25 times of O/C value than AB-C coal, and its water holding capacity at primary adsorption stage (~1.086 mmol/g) is ~ 3.73 times than the latter one (~0.291 mmol/g). The above observations confirmed that the positive correlations between the oxygen containing degree and the maximum water holding capacity during the primary adsorption stage. The results also confirmed that even the water molecules firstly adsorbed on the coal surface sites but strictly the primary adsorption sites should be hydrophilic centers such as oxygen-containing functional groups, rather than all the surface sites. The results implicitly illustrate that the pore surface area may not be the determining parameter that controls water vapor sorption at least during the primary adsorption stage. However, the statement for the total water holding capacity should be carefully extrapolated without further analyzing the secondary adsorption stage.

Based on the phenomenological Dubinin-Serpinsky approach, the secondary adsorption capacity of water vapor is quantified in in Eq.2. The total amount of water vapor uptake combing the primary and secondary adsorptions can be calculated by Eq.3. To evaluate the factors influencing the secondary adsorption, the contribution of secondary adsorption on total sorption isotherm can be computed by subtracting the primary adsorption quantity (Eq.1) from Eq.3. For simplification, we used the maximum primary adsorption amount (m_L) quantified theoretically to represent the contribution of primary adsorption to the total water vapor uptake in this study. Taking 30°C for example, as shown in Tab.2, the primary adsorption capacity for IL-C#1 and IL-C#2 and AB-C coal are estimated as 1.330 mmol/g, 1.347 mmol/g, and 0.293 mmol/g. If we examined the total water vapor uptake at relative humidity of 95%, these three coal samples have the adsorbed amounts of water vapor of 9.220 mmol/g, 4.550 mmol/g, and 0.788 mmol/g. Correspondingly, the modeled amounts of secondary adsorptions in these three coal samples at this relative humidity are about 7.890 mmol/g, 3.203mmol/g and 0.495mmol/g. For both IL-C#1 and IL-C#2, they almost have the similar primary adsorption capacities, but the secondary adsorption constituting by the formation of water clusters or even pore filling show an apparent difference and IL-C#1 is estimated to be

2.46 times of IL-C#2. The secondary adsorption process accommodating both formation of water cluster and/or pore filling intrinsically occurs within the confined space provided by the pore structure/network. Thus, the PSD and the pore volume can influence the uptake process of water vapor. The cumulative pore volume of IL-C#1 is ~ 0.0137cm^3/g based on the DFT theory, which is about 9.79 times than that of IL-C#2 does (0.0014cm^3/g). Here the pore volume difference between these two coal samples shows positive relationship with their water holding capacities (~ 2.46 times difference). By comparing the secondary adsorption results between IL-C#2 and AB-C coal, IL-C#2 (3.203mmol/g) is about 6.47 times than that of the AB-C (0.495mmol/g). Interestingly, the cumulative pore volume for pore sizes determined by liquid nitrogen adsorption in IL-C#2 (0.0014cm^3/g) is almost same with that in AB-C (0.002 cm^3/g). The results between IL-C#2 and AB-C demonstrate that the cumulative pore volume is not the decisive factor influencing the amount of secondary adsorption for these two coal samples, which implicitly elaborates the underlying mechanism that the primary adsorption plays a decisive role in determining the sorption centers for the formation of water clusters during the secondary adsorption stage.

Based on the modeling regressed results of m_L, R_L and c, the contributions of primary and secondary adsorptions to the total adsorption isotherm were calculated and plotted with respect to water vapor pressure in Fig.8 (a2), (b2) and (c2). Under the same temperature, the results shown that the primary adsorption non-linearly increases with vapor pressure increases but the primary adsorption will reach its maximum capacity, which is controlled by Eq.1. Simultaneously, the secondary adsorption will start after the monomolecular coverage is achieved during the primary adsorption stage. At relatively lower relative humidity, the primary adsorption dominates the process of water vapor uptake, while the secondary adsorption will play the decisive role in determining the final/total equilibrium amount of water vapor adsorption at high relative humidity. It is apparent that the temperature has considerable influence on the entire process. More precisely, as the increase of temperature, the movement of water molecule is enhanced resulting in that partial water molecules have enough energy to get rid of the attraction force between water molecules. The escaped water molecules decrease moisture amount at the given equilibrium relative humidity. At the same time, the higher temperature has limited effects on primary adsorption process, which

is mainly due to the stronger chemical H-binding energy cannot be overcame by the increase molecular energy.

5.2.3 Coal-water interaction process derived from isosteric heat of adsorption

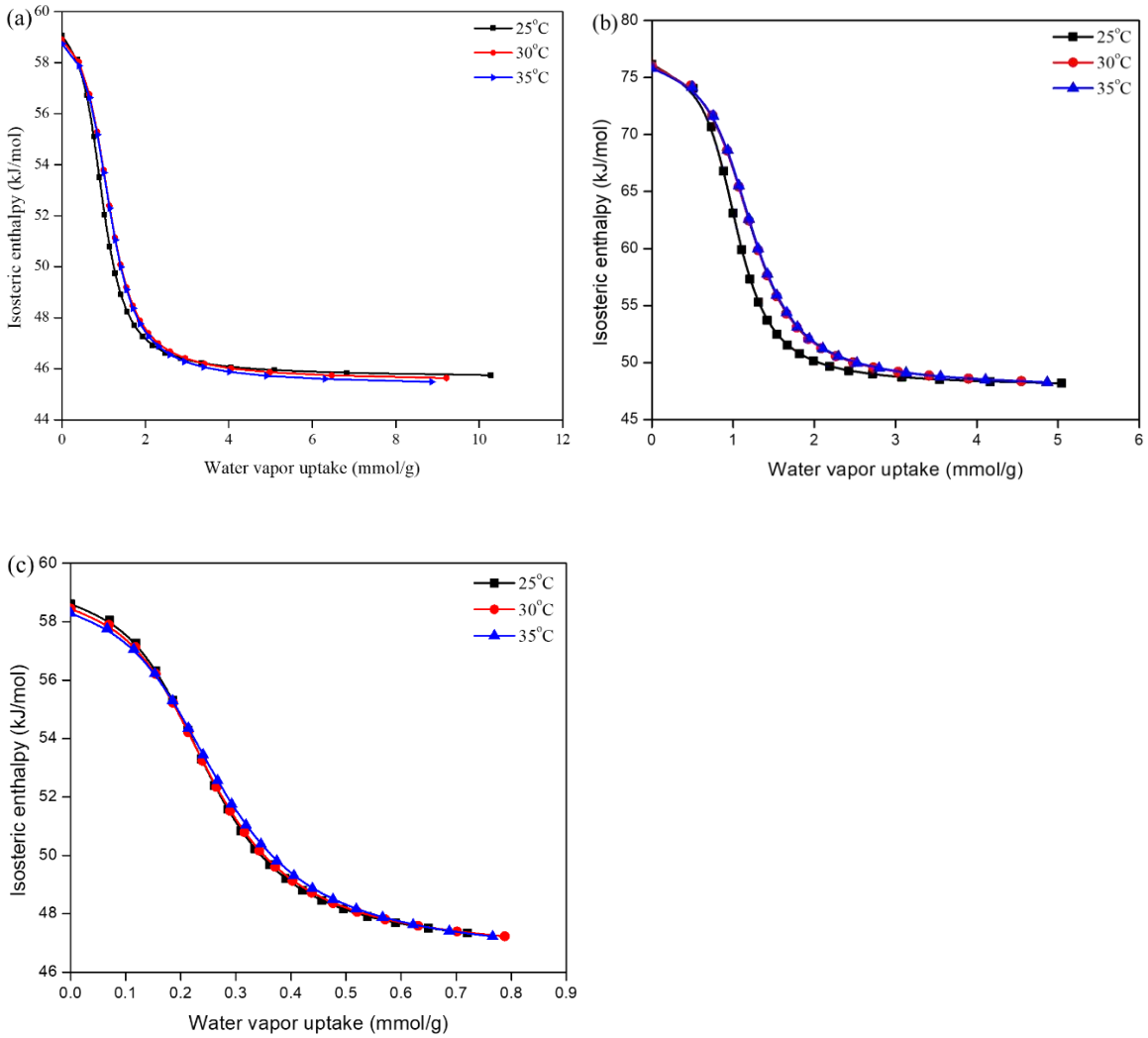

Fig.9: Isosteric heat of adsorption of water vapor in IL-C#1

Previous studies shown that thermodynamically adsorption is an exothermic process and the sorption capacity decreases with increasing temperature because of a higher ordered adsorbed state [12]. The isosteric heat of adsorption depends on the surface chemistry and the pore structure. The isosteric heat of water vapor adsorption can be used to evaluate the energy of interaction or intermolecular bonding between water molecules and solid surfaces. For water vapor sorption on coal, the presence of oxygen-

containing functional provides higher energetic sorption sites, which are preferentially occupied by water molecules. The strong hydrogen bonding energy between the functional groups and water molecules can produce higher isosteric heat of sorption by comparing with the latent heat of bulk water condensation (45 kJ/mol at a surface coverage up to 10%). In this study, the isosteric heat of sorption was estimated by Eq. (13). The parameters q_L and q_0 were fitted based on Eqs. (9) and (10), and the modeled data in Tab. (2). Based on Eq. (13), the isosteric heats of sorption for these three samples were plotted in Fig.9. The isosteric heats of adsorption decrease as water vapor uptake increase for all the samples, and as such represents an exothermic process. Taking the temperature of 25℃ for example, the isosteric heats of adsorption for IL-C#1 and IL-C#2, and AB-C range from ~59.1 to 45.7 kJ/mol, from ~76.2 to 48.2 kJ/mol, 58.6 to 47.3 kJ/mol as water vapor uptakes increase, respectively. At lower water adsorption uptake, the hydrogen bonding energy between the water molecules and solid matrix surface is strong and the isosteric heat of sorption is expected to be high at this stage, as illustrated in Fig.9. In Fig.9, as the increase of relative humidity, water molecules adsorb in the less active sites and multilayer adsorption occurs. The corresponding isosteric heat of water adsorption was found to have values very close to the latent heat of bulk water condensation. At a specified water adsorption uptake, the temperature difference can result in a small shift on the isosteric heat of adsorption curves, which is mainly due to the effects of temperature on the hydrogen bonding energy between the water molecules and solid matrix surface, and the interaction energy between water molecules.

6. Discussion on colloidal gel structure of coal-water system as a function of relative humidity

6.1. Physical changes on colloidal gel structure of coal-water system

Based on the experimental and modeling results in Sections 3 and 4 as well as previous studies, moisture can be held in coals in several distinct forms mainly including sorbed water, capillary condensed water, and superficial free water [67-70]. Coal has a colloidal gel-like structure [69, 71-73] and coal-water system may be viewed as a colloidal gel that can shrink and swell in response to moisture loss or gain is well established and studied [72-74]. Fig.10 shows the volumetric phase distribution of coal-water system

as a function of relative humidity. The diagram ideally applies to relative volume changes on colloidal gel structure of coal-water system from initial dry condition (0 relative humidity) to the normal saturated condition (100% relative humidity). At the initial dry condition (point A), the coal-water system only contains dry solid coal matrix and open porosity volume. As relative humidity increases, moist air enters/fills the open fracture/pore space and almost simultaneously partial water molecules are held by hydrogen-bonding sites on the solid matrix surface in adsorbed phase (point B). As the relative humidity continuously increases, those adsorbed water molecules occupied on primary sites are considered as the secondary centers for the formation of water aggregates or clusters. Also, water in capillary condensed phase will be formed in narrow pores at relatively high relative humidity condition (point C). Due to the limited pore space in coal, the coal-water system will arrive at the normal equilibrium state (point D) at the normal 100% relative humidity. From Fig.10, it is worth noting that the solid coal matrix will swell to some extent in response to moisture gain due to the colloidal gel-like structure of coal. To what extent are the physical changes on colloidal gel structure of coal-water system as a function of relative humidity is of practical significance.

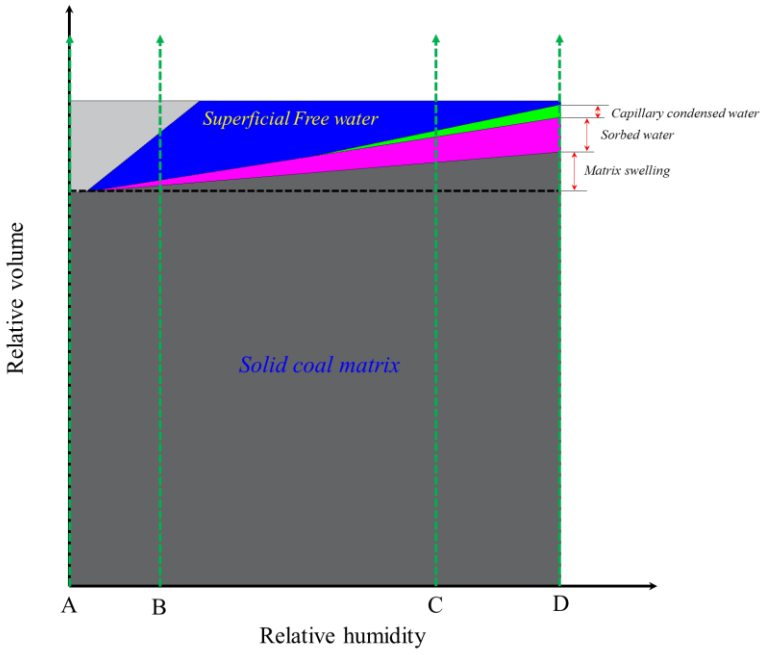

Fig.10: Volumetric phase distribution of solid coal matrix and distinct forms of moisture as a function of relative humidity

Deevi and Suuberg studied the physical changes accompanying drying of western U.S. lignites [69]. The water desorption-adsorption isotherms were plotted in Fig. (11). In Fig.11(a) and (b), the Gascoyne and Freedom lignites show some irreversibility in the desorption-adsorption cycle. This was also observed for sub-bituminous coal samples in Fig.6 (a1) and (b1) in this study. Fig.6 (a1) and (b1) shown that the adsorption-desorption cycles on dried coals (the first step of DVS test is drying condition, as shown in Fig.(3)) and it was observed that the loops are closed at both the high and low ends of the relative humidity scale. However, in Fig.11(a) and (b), the desorption-adsorption cycle begun with fresh coal fails to close at high end of the relative humidity scale. Behind the phenomenon is the evidence of an irreversible change in coal structure during initial drying stage. In addition, the effect of drying on the structure of a sub-bituminous coal was also studied by Gorbaty [74]. The results shown that drying sub-bituminous coal has a marked effect on its physical structure - the sub-bituminous coal exhibits collapse behavior and some collapsed are irreversible, which results in decreased mass transport through coal particle.

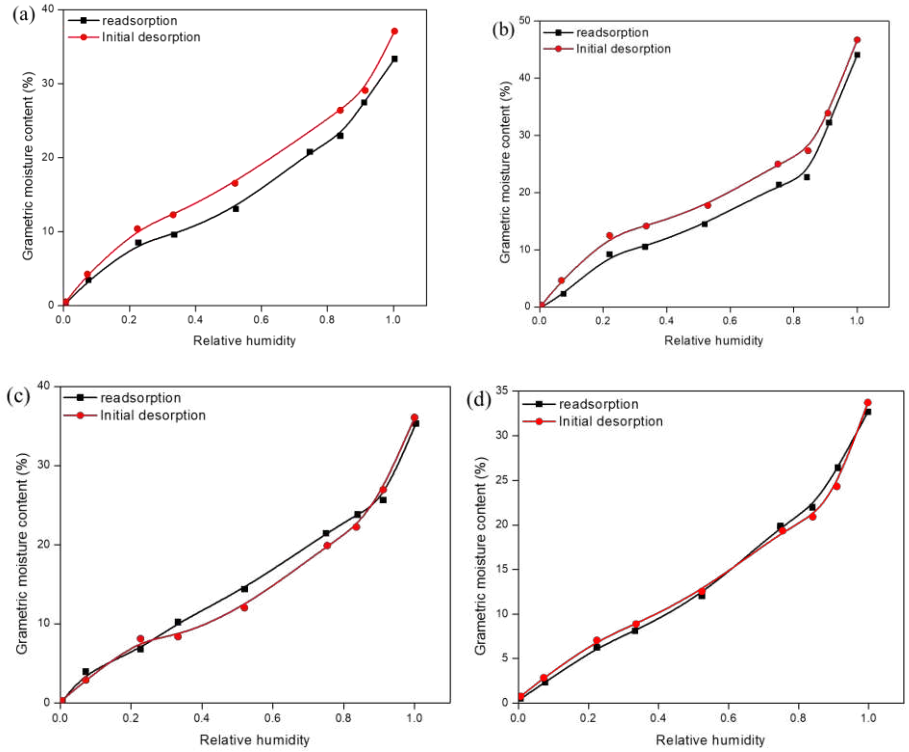

Fig.11: Water desorption-readsorption isotherms of North Dakota lignites as a function of relative humidity [69]. (a) Freedom sample. (b) Gascoyne sample. (c) Glenn Harold sample. (d) Beulah sample.

To further study the pore collapse behavior upon drying, Deevi and Suuberg further measured the macroscopic shrinkages on larger cubic lignite samples from North Dakota [69]. Subsequently, they compared the measured macroscopic shrinkages and the volumetric shrinkages calculated on the assumption that all pores are initially filed with water and any water removed has a specific volume of 1 cm^3/g, as shown in Fig.12. It was apparent that for all samples there are at least some regions of relative humidity in which collapse occurs to an extent much greater than predicted only removal of bulk water.

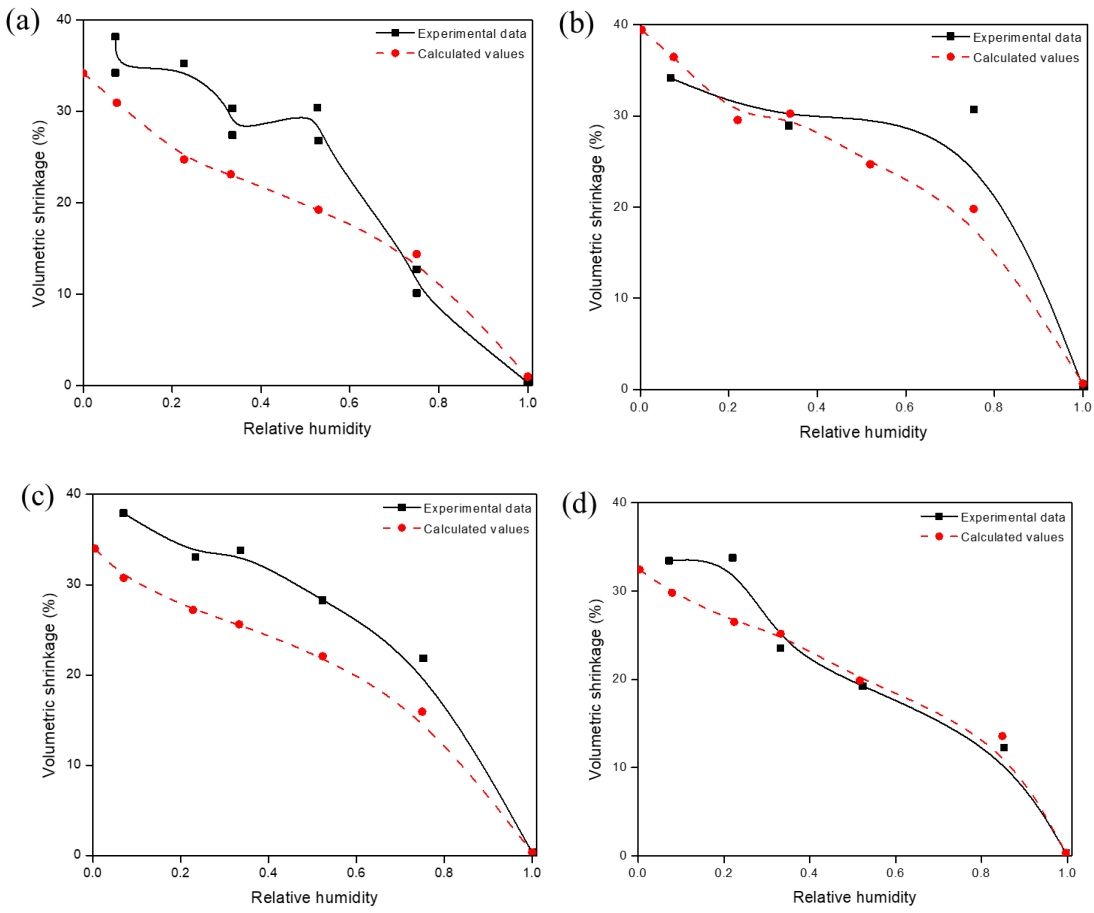

Fig.12: Volumetric shrinkage of North Dakota lignites as a function of relative humidity [69]. (a) Freedom sample. (b) Gascoyne sample. (c) Glenn Harold sample. (d) Beulah sample.

Also, Deevi and Suuberg measured the volumetric reswelling on dried finely ground lignites based on the conventional solvent swelling technique [69]. It shown that the shrinkages of all the four samples upon drying are only partly reversible. The irreversibility of the process manifests itself even during partial drying (to relative humidity = 0.75). Based on Kelvin equation and using the assumption of perfect wetting

of the pore walls by water, the pores with diameter of ~7 nm and larger at relative humidity of 0.75 are involved in the pore collapse scenario, which thus implies that irreversible shrinkage of the lignite samples is associated mainly with collapse of macroporosity and transitional porosity [69].

6.2. Thermodynamics accompanying colloidal gel structure swelling/shrinkage

The thermodynamics of the coal-water swelling process should consider various correlations of swellability with water properties [73]. Suuberg et al. studied the solvent swelling thermodynamics of lignite in specifically interacting solvents [73]. The results shown that the swelling property of coals is strongly determined by the electron-donating capacity of the solvents. Also, the swelling correlates with the heat of immersion of coals in solvents, and thus it appears that it is the enthalpy of interaction of specifically interacting solvents with surface functionalities in coal that mainly determines swelling behavior. There is generally a particular number of specific interaction sites in the coal that determine the maximum extent of swelling, though there is the possibility of nonspecific interactions contributing to further swelling, beyond this "titration end point" [73]. In this study, it can be concluded from Section 5.2.3 that the isosteric heat of water adsorption decreases as water vapor uptake increases, which was found to be close to the latent heat of bulk water condensation at higher relative humidity. The results confirmed that the primary adsorption is controlled by the stronger bonding energy while the interaction energy between water molecules during secondary adsorption stage is relatively weak. Thus, the fact that the coal structure undergoes what might be considered a "solvent swelling" in water means that the thermodynamics are complicated by the fact that internal bonding interactions within the coal are disrupted at the same time as new bonding interactions take place with the water molecules.

7. Summary and conclusions

We conducted the coal and water vapor interaction experiment to investigate the water vapor sorption behavior of various coals. The relationships between water vapor sorption capacity and the surface chemistry of coal and coal pore structure were discussed in detail. Theoretically, a mechanism-based isotherm model was proposed to estimate the water vapor uptake at various relative humidity/water vapor

pressure. Simultaneously, the isosteric heat of water vapor sorption is modeled and determined by combining the Clausius-Clapeyron equation. The following major conclusions can be summarized:

1) Oxygen containing surface features of coal matrix was quantified by O/C ratio through XPS technique. IL-C#2 has the highest oxygen containing degree (0.18) among three tested samples, followed by IL-C#1 (0.13), and the minimum is AB-C coal of 0.04.
2) BET, SSA, PSD and cumulative pore volume were evaluated through low temperature nitrogen adsorption. The cumulative pore volumes for the three samples were 0.0137 cm^3/g, 0.0014 cm^3/g and 0.002 cm^3/g, respectively. IL-C#1 has highest SSA (8.032 m^2/g), followed by IL-C#2 (0.49m^2/g) and AB-C (1.12 m^2/g).
3) The isotherm model of water vapor sorption was proposed and validated. The validated model was used to distinguish the contributions of primary and secondary sorption to the apparent water vapor sorption at different relative humidity ranges.
4) SSA of coal is not the determining parameter that controls water vapor sorption at least during the primary adsorption stage. Oxygen containing degree dominates the primary adsorption, and togethering with the cumulative pore volume determine the secondary adsorption. Higher temperature has limited effects on primary adsorption process, which is mainly due to the stronger chemical H-binding energy is the energy barrier for water molecule detachment at high temperature.
5) The isosteric heat of water adsorption decreases as water vapor uptake increases, which was found to be close to the latent heat of bulk water condensation at higher relative humidity. The results confirmed that the primary adsorption is controlled by the stronger bonding energy while the interaction energy between water molecules during secondary adsorption stage is relatively weak.
6) Coal has a shrinkage/swelling colloidal structure with moisture loss/gain and it exhibits collapse behavior and some collapse are irreversible, which plays a significant role in determining moisture retention. The thermodynamics within coal-water interactions are complicated since internal bonding interactions within the coal are disrupted at the same time as new bonding interactions take place with the water molecules.

Declaration of Competing Interest

The authors declare that they have no known competing financial interests or personal relationships that could have appeared to influence the work reported in this paper.

Acknowledgement

This study was sponsored by the Open Fund Project Funded by State Key Laboratory of Coal Mine Disaster Dynamics and Control, Chongqing University (Grant #2011DA105287-FW201903). We also want to thank the China Scholarship Council (CSC) for the financial support (Grant #201806430028).

References

[1] Smith JA, Ramandi HL, Zhang C, Timms W. Analysis of the influence of groundwater and the stress regime on bolt behaviour in underground coal mines. Int J Coal Sci Technol 2019;6:286–300.

[2] Fan L, Ma L, Yu Y, Wang S, Xu Y. Water-conserving mining influencing factors identification and weight determination in northwest China. Int J Coal Sci Technol 2019;6:95–101.

[3] Fan L, Ma X. A review on investigation of water-preserved coal mining in western China. Int J Coal Sci Technol 2018;5:411–6.

[4] Li W, Wang Q, Liu S, Pei Y. Study on the creep permeability of mining-cracked N2 laterite as the key aquifuge for preserving water resources in Northwestern China. Int J Coal Sci Technol 2018;5:315–27.

[5] Furmaniak S, Gauden PA, Terzyk AP, Rychlicki G. Water adsorption on carbons - Critical review of the most popular analytical approaches. Adv Colloid Interface Sci 2008;137:82–143.

[6] Huang Q, Liu S, Wang G, Wu B, Yang Y, Liu Y. Gas sorption and diffusion damages by guar-based fracturing fluid for CBM reservoirs. Fuel 2019;251:30–44.

[7] Huang Q, Liu S, Wang G, Wu B, Zhang Y. Coalbed methane reservoir stimulation using guar-based fracturing fluid: A review. J Nat Gas Sci Eng 2019;66:107–25.

[8] Yang Y, Liu S. Laboratory study of cryogenic treatment induced pore-scale structural alterations of Illinois coal and their implications on gas sorption and diffusion behaviors. J Pet Sci Eng 2020;194:107507.

[9] Tang X, Ripepi N, Valentine KA, Keles C, Long T, Gonciaruk A. Water vapor sorption on Marcellus shale: measurement, modeling and thermodynamic analysis. Fuel 2017;209:606–14.

[10] Yu J, Tahmasebi A, Han Y, Yin F, Li X. A review on water in low rank coals: The existence, interaction with coal structure and effects on coal utilization. Fuel Process Technol 2013;106:9–20.

[11] Liu A, Liu S, Wang G, Sang G. Modeling of Coal Matrix Apparent Strains for Sorbing Gases Using a Transversely Isotropic Approach. Rock Mech Rock Eng 2020.

[12] Busch A, Gensterblum Y. CBM and CO2-ECBM related sorption processes in coal: A review. Int J Coal Geol 2011;87:49–71.

[13] Mahajan OP, Walker PL. Water adsorption on coals. Fuel 1971;50:308–17.

[14] Allardice DJ, Evans DG. The-brown coal/water system: Part 2. Water sorption isotherms on bed-moist Yallourn brown coal. Fuel 1971;50:236–53.

[15] Joubert JI, Grein CT, Bienstock D. Effect of moisture on the methane capacity of American coals. Fuel 1974;53:186–91.

[16] Kaji R, Muranaka Y, Otsuka K, Hishinuma Y. Water absorption by coals: effects of pore structure and surface oxygen. Fuel 1986;65:288–91.

[17] McCutcheon AL, Barton WA, Wilson MA. Characterization of water adsorbed on bituminous coals. Energy and Fuels 2003;17:107–12.

[18] Charrière D, Behra P. Water sorption on coals. J Colloid Interface Sci 2010;344:460–7.

[19] Švábová M, Weishauptová Z, Přibyl O. Water vapour adsorption on coal. Fuel 2011;90:1892–9.

[20] Kadioğlu Y, Varamaz M. The effect of moisture content and air-drying on spontaneous

combustion characteristics of two Turkish lignites. Fuel 2003;82:1685–93.

[21] Ahamed MAA, Perera MSA, Matthai SK, Ranjith PG, Dong-yin L. Coal composition and structural variation with rank and its influence on the coal-moisture interactions under coal seam temperature conditions – A review article. J Pet Sci Eng 2019;180:901–17.

[22] Sang G, Liu S, Elsworth D. Water Vapor Sorption Properties of Illinois Shales Under Dynamic Water Vapor Conditions: Experimentation and Modeling. Water Resour Res 2019;55:7212–28.

[23] Zhang Y, Jing X, Jing K, Chang L, Bao W. Study on the pore structure and oxygen-containing functional groups devoting to the hydrophilic force of dewatered lignite. Appl Surf Sci 2015;324:90–8.

[24] Mu, R., Malhotra VM. A new approach to elucidate coal-water interactions by an in situ transmission FT-i.r. technique. Fuel 1991;70:1233–5.

[25] Suárez N, Laredo E, Nava R. Characterization of four hydrophilic sites in bituminous coal by ionic thermal current measurements. Fuel 1993;72:13–8.

[26] van Krevelen DW. Coal: Typology-Physics-Chemistry-Constitution. Elsevier 1993:1002.

[27] Schafer HNS. Carboxyl groups and ion exchange in low-rank coals. Fuel 1970;49:197–213.

[28] Giroux L, Charland JP, MacPhee JA. Application of thermogravimetric Fourier transform infrared spectroscopy (TG-FTIR) to the analysis of oxygen functional groups in coal. Energy and Fuels 2006;20:1988–96.

[29] Murata S, Hosokawa M, Kidena K, Nomura M. Analysis of oxygen-functional groups in brown coals. Fuel Process Technol 2000;67:231–43.

[30] Ogunsola OI. Thermal upgrading effect on oxygen distribution in lignite. Fuel Process Technol 1993;34:73–81.

[31] Stach E. Stach's Textbook of Coal Petrology 1982.

[32] Brennan, J. K.; Bandosz, T. J.; Thomson, K. T.; Gubbins KE. Water in porous carbons. Colloids and surfaces. Physico- Chem Eng Asp 2001;187:187–8, 539–68.

[33] Ward CR. Analysis and significance of mineral matter in coal seams. Int J Coal Geol

2002;50:135–68.

[34] Ward CR. Analysis, origin and significance of mineral matter in coal: An updated review. Int J Coal Geol 2016;165:1–27.

[35] Susilawati R, Ward CR. Metamorphism of mineral matter in coal from the Bukit Asam deposit, south Sumatra, Indonesia. Int J Coal Geol 2006;68:171–95.

[36] Tiwari B, Ajmera B. Consolidation and swelling behavior of major clay minerals and their mixtures. Appl Clay Sci 2011;54:264–73.

[37] Bolt GH. Physico-chemical analysis of the compressibility of pure clays. Geotechnique 1956;6:86–93.

[38] Langmuir I. The constitution and fundamental properties of solids and liquids. Part I. Solids. J Am Chem Soc 1916;38:2221–95.

[39] Brunauer S, Emmett PH, Teller E. Adsorption of Gases in Multimolecular Layers. J Am Chem Soc 1938;60:309–19.

[40] Anderson RB. Modifications of the Brunauer, Emmett and Teller Equation. J Am Chem Soc 1946;68:686–91.

[41] de Boer JH. The dynamical character of adsorption. 1953.

[42] Guggenheim EA. Applications of statistical mechanics. 1966.

[43] Dubinin MM, Zaverina ED SV. Trans Faraday Soc 1955:1760.

[44] Dubinin MM SV. Doklady AN SSSR[in Russian] 1981;285:1151.

[45] Barton SS, Evans MJB, MacDonald JAF. The adsorption of water vapor by porous carbon. Carbon N Y 1991;29:1099–105.

[46] D'Arcy RL, Watt IC. Analysis of sorption isotherms of non-homogeneous sorbents. Trans Faraday Soc 1970;66:1236–45.

[47] Malakhov AO VV. Polym Sci Ser A 2000;42:1120.

[48] Thommes M, Kaneko K, Neimark AV, Olivier JP, Rodriguez-Reinoso F, Rouquerol J et al. Physisorption of gases, with special reference to the evaluation of surface area and pore size

distribution (IUPAC Technical Report). Pure Appl Chem 2015;87:1051–69.

[49] Do DD, Do HD. Model for water adsorption in activated carbon. Carbon N Y 2000;38:767–73.

[50] Liu L, Tan S (Johnathan), Horikawa T, Do DD, Nicholson D, Liu J. Water adsorption on carbon - A review. Adv Colloid Interface Sci 2017;250:64–78.

[51] Kraehenbuehl F, Quellet C, Schmitter B, Stoeckli HF. The relationship between immersion calorimetry and the parameters of the water adsorption isotherm on active carbons. J Chem Soc Faraday Trans 1 Phys Chem Condens Phases 1986;82:3439–45.

[52] Mahajan OP. CO2 surface area of coals: The 25-year paradox. Carbon 1991;29(6):735–42.

[53] Dacey JR, Clunie JC, Thomas DG. The adsorption of water by Saran charcoal. Trans Faraday Soc 1958;54:250–6.

[54] Wan K, He Q, Miao Z, Liu X, Huang S. Water desorption isotherms and net isosteric heat of desorption on lignite. Fuel 2016;171:101–7.

[55] Kovtun A, Jones D, Dell'Elce S, Treossi E, Liscio A, Palermo V. Accurate chemical analysis of oxygenated graphene-based materials using X-ray photoelectron spectroscopy. Carbon 2019;143:268–75.

[56] Zaldivar RJ, Adams PM, Nokes J, Kim HI. Surface functionalization of graphenelike materials by carbon monoxide atmospheric plasma treatment for improved wetting without structural degradation degradation. Journal of vacuum science and technology B 2017;107.

[57] Behm RJ. Interaction of a Self-Assembled Ionic Liquid Layer with Graphite(0001): A Combined Experimental and Theoretical Study. Physical chemistry letters 2016.

[58] Seah MP. Summary of ISO / TC 201 Standard : VII ISO 15472 : 2001- surface chemical analysis - x-ray photoelectron spectrometers - calibration of energy scales 2001:721–3.

[59] Gregg, S.J., Sing KSW. Adsorption Surface Area and Porosity. 2nd edition. Acad Press New York 1982:303.

[60] Sang G, Liu S, Zhang R, Elsworth D, He L. Nanopore characterization of mine roof shales by SANS, nitrogen adsorption, and mercury intrusion: Impact on water adsorption/retention behavior.

Int J Coal Geol 2018;200:173–85.

[61] Nishino J. Adsorption of water vapor and carbon dioxide at carboxylic functional groups on the surface of coal. Fuel 2001;80:757–64.

[62] Barton SS, Evans MJB, MacDonald JAF. Adsorption of Water Vapor on Nonporous Carbon 1994:4250–2.

[63] Freeman GB, Reucroft PJ. Adsorption of HCN and H_2O vapor mixtures by activated and impregnated carbons. Carbon 1979;17:313–6.

[64] Tarasevich YI, Aksenenko E V. Interaction of water, methanol and benzene molecules with hydrophilic centres at a partially oxidised model graphite surface. Colloids Surfaces A Physicochem Eng Asp 2003;215:285–91.

[65] Alduchov OA, Eskridge RE, Climatic N, Oceanic N. Improved Magnus form approximation of saturation vapor pressure. J Appl Meteorol 1996;35:601–9.

[66] Allardke DJ, Evans DG. Fart 2 . Water sorption isotherms on bed-moist Yallourn brown coal. Fuel 1971;50 (3):236–53.

[67] Maroulis ZB, Tsami E, Marinos-Kouris D, Saravacos GD. Application of the GAB model to the moisture sorption isotherms for dried fruits. J Food Eng 1988;7:63–78.

[68] Kube WR. Sorption of water vapor by thermally treated lignite at different relative humidities. Ind Eng Chem, Eng Data Ser 1957;2:46–51.

[69] Deevi SC, Suuberg EM. Physical changes accompanying drying of western US lignites. Fuel 1987;66:454–60.

[70] Choi JG, Do DD, Do HD. Surface diffusion of adsorbed molecules in porous media: Monolayer, multilayer, and capillary condensation regimes. Ind Eng Chem Res 2001;40:4005–31.

[71] Suuberg EM. Comments regarding the use of coal swelling to count hydrogen-bond cross-links in coals. Energy and Fuels 1997;11:1103–4.

[72] Suuberg EM, Otake Y, Yun Y, Deevi SC. Role of moisture in coal structure and the effects of drying upon the accessibility of coal structure. Energy and Fuels 1993;7:384–92.

[73] Suuberg EM, Otake Y, Langner MJ, Leung KT, Milosavljevic I. Coal macromolecular network structure analysis: solvent swelling thermodynamics and its implications. Energy and Fuels 1994;8:1247–62.

[74] Gorbaty ML. Effect of drying on the adsorptive properties of subbituminous coal. Fuel 1978;57:796.

Figures

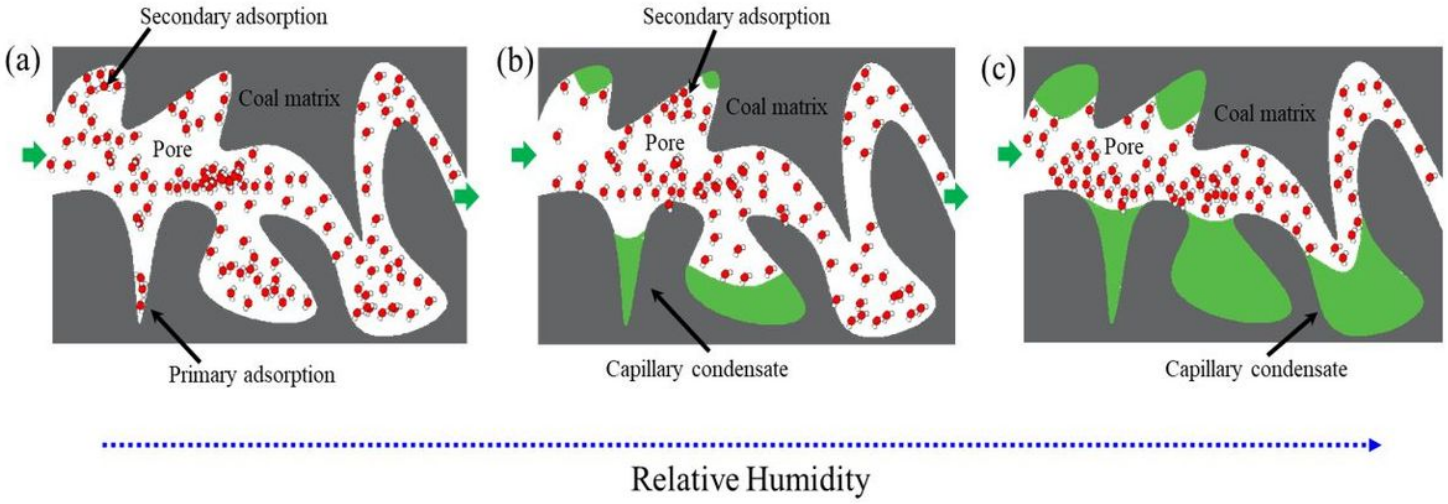

Figure 1

Schematic of water vapor adsorption mechanisms in coal with increasing relative humidity (modified from Sang et al.[22]). (a) Primary adsorption on hydrophilic sites induced by monolayer adsorption dominates at initial low relative humidity. (b) and (c) Secondary adsorption dominates at higher relative humidity including formation of multilayer adsorption and capillary condensation.

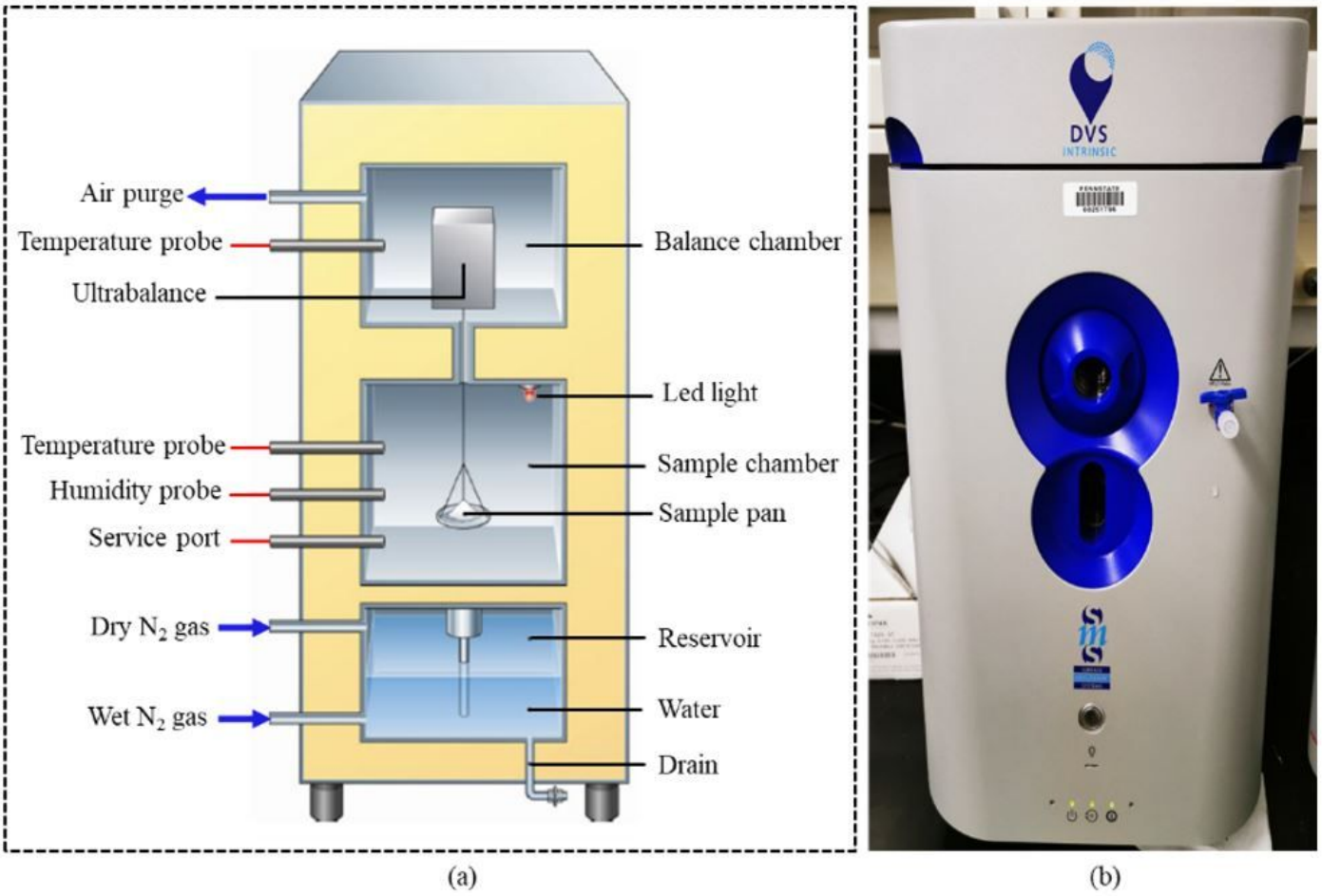

Figure 3

Schematic and lab-view of the DVS instrument

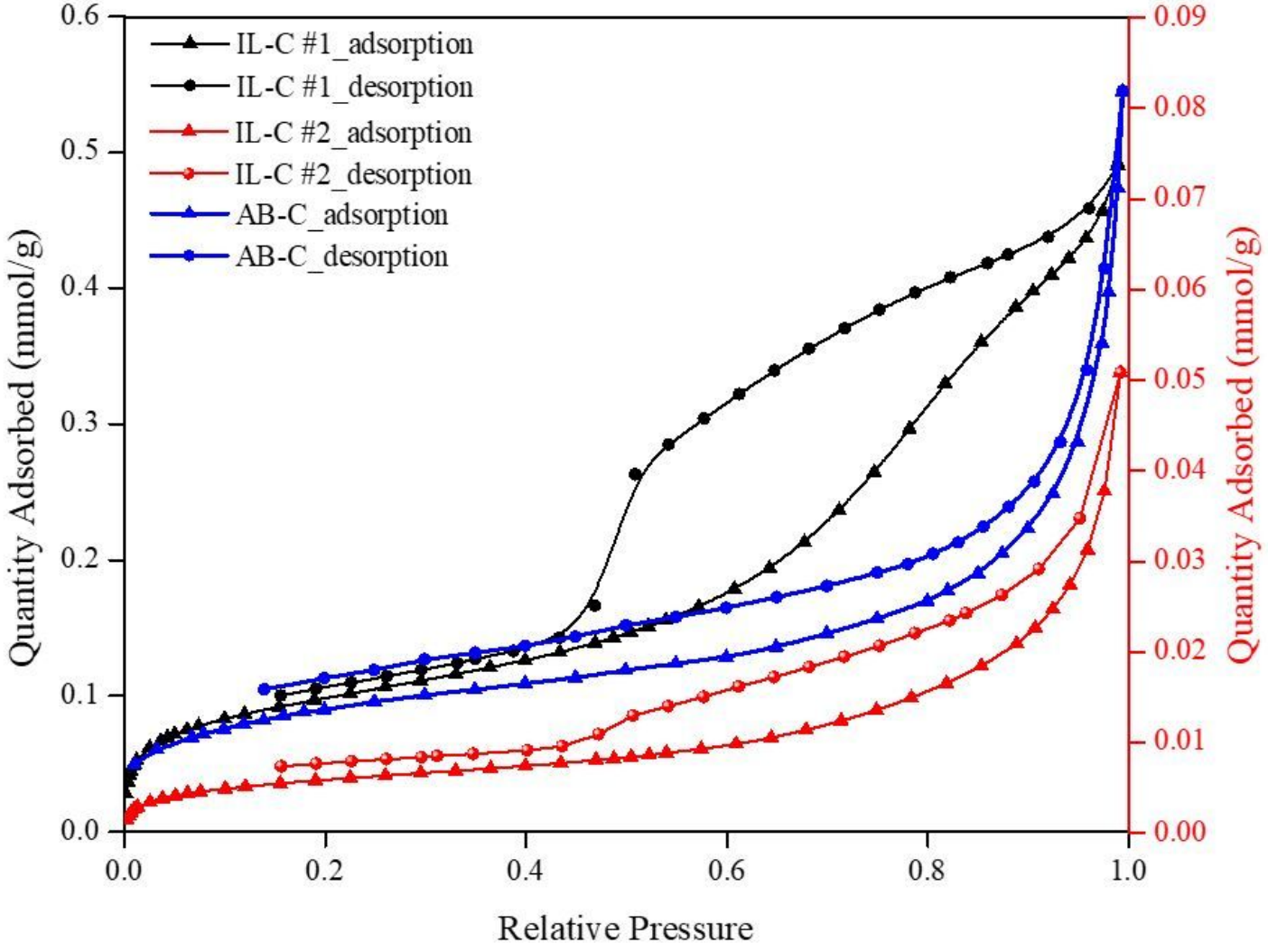

Figure 4

Low-temperature nitrogen adsorption isotherms

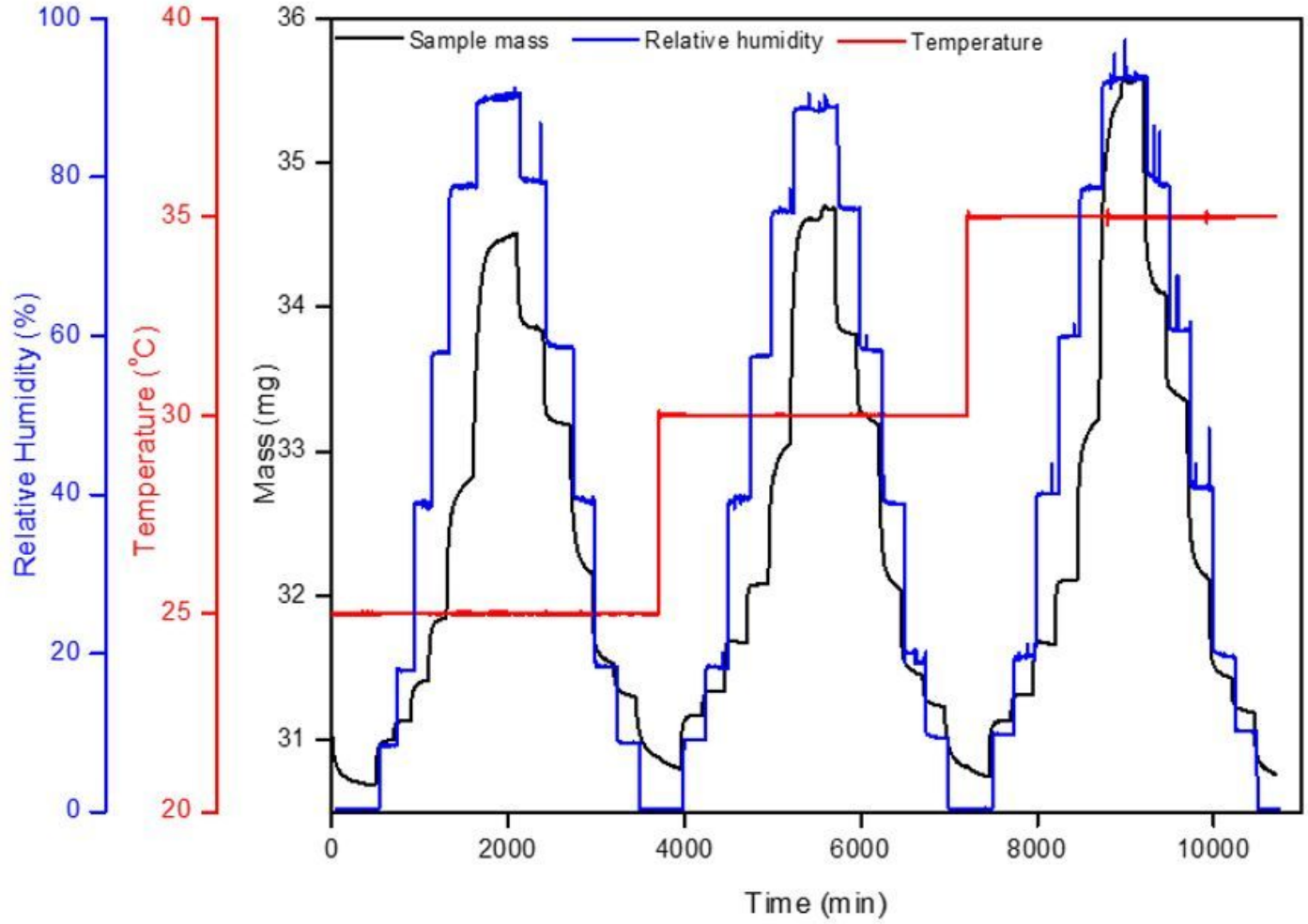

Figure 4

Three full circles of water vapor sorption measurements - raw data from DVS instrument dynamic vapor sorption analyzer for IL-C#1

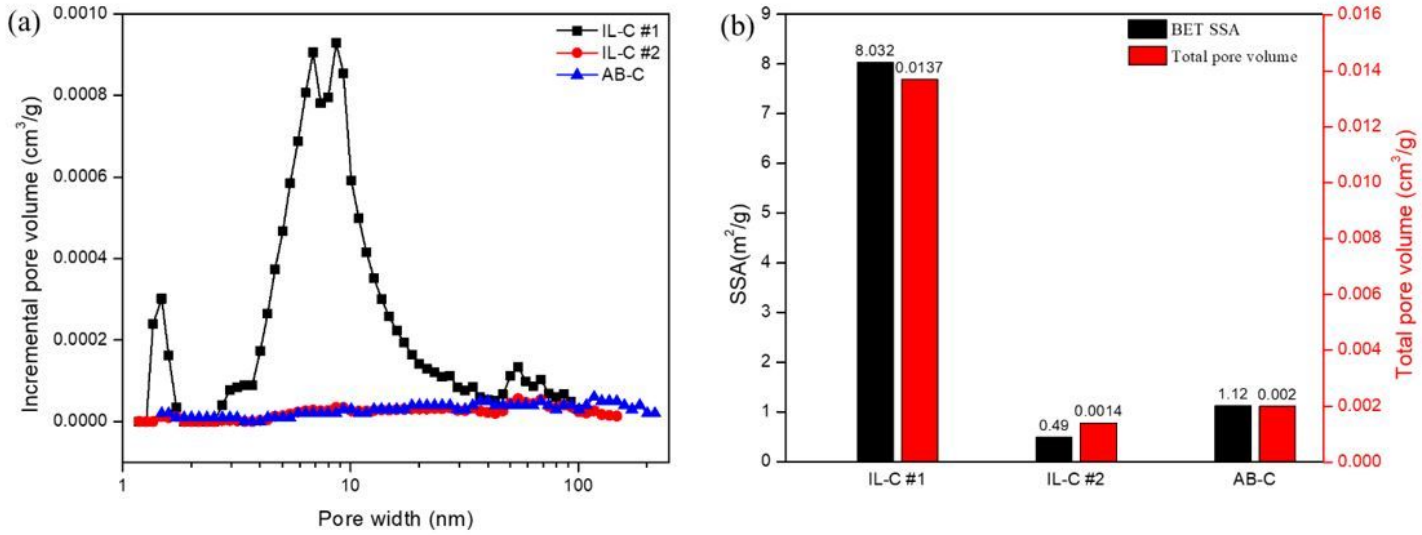

Figure 5

Pore properties based on BET model and density functional theory. (a) Pore size distribution and (b) BET SSA and cumulative pore volume

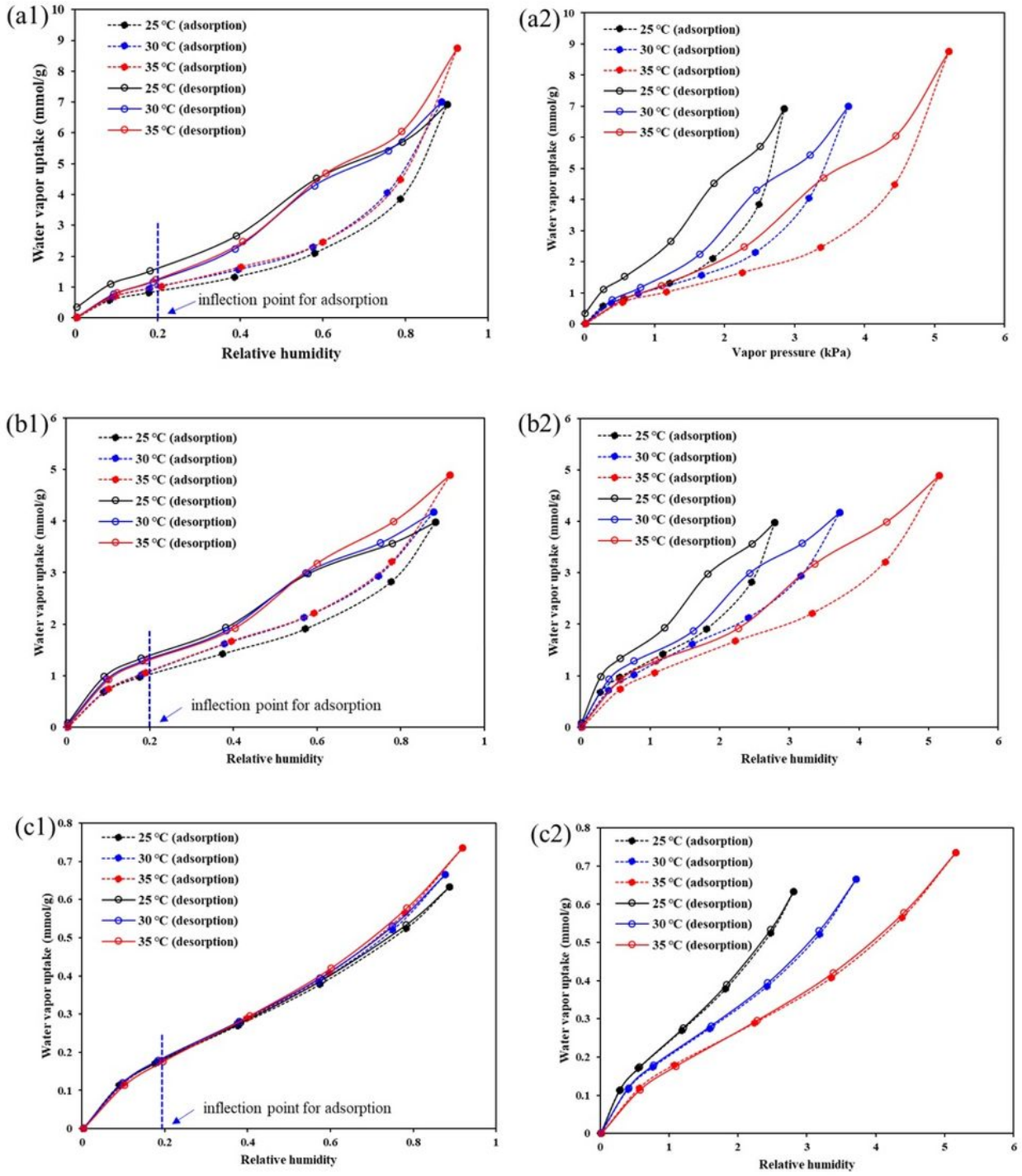

Figure 7

Water ad/desorption isotherms with respect to relative humidity/vapor pressure: (a1) and (a2) IL-C#1 sample; (b1) and (b2) IL-C#2 sample; (c1) and (c2) AB-C sample

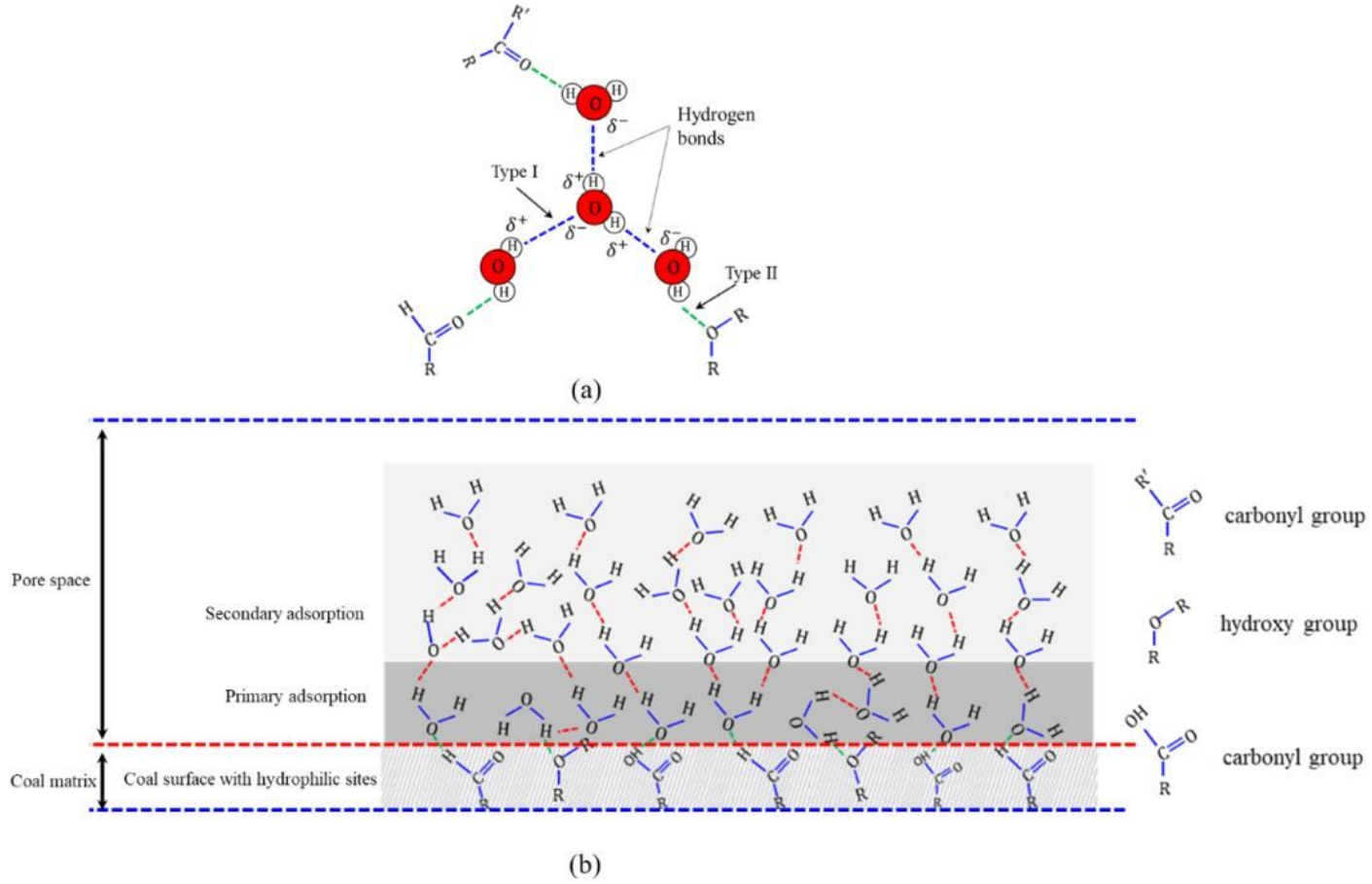

Figure 7

Hydrogen bonds of primary adsorption on coal surface with hydrophilic sites and secondary adsorption formed on primary centers.

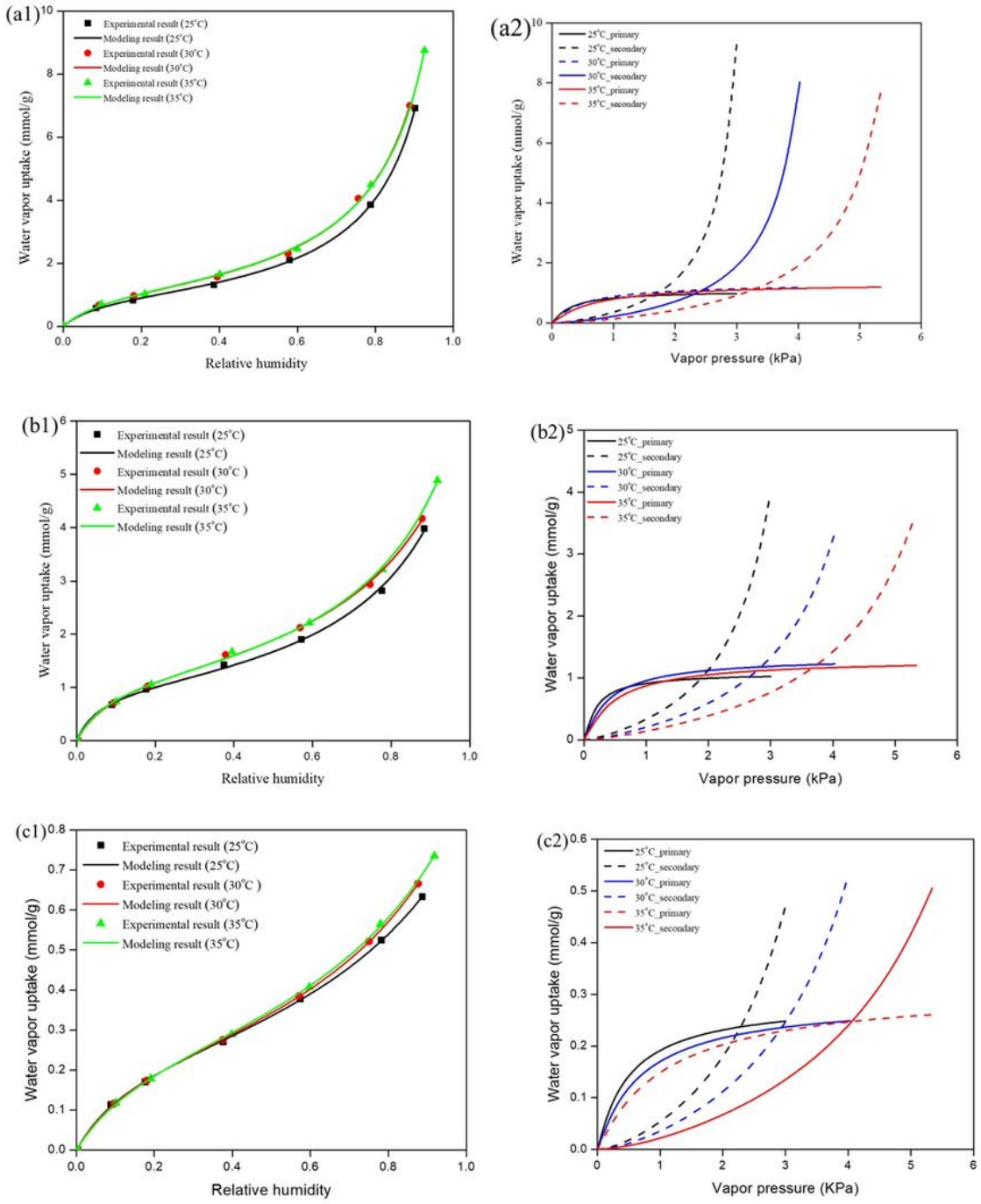

Figure 8

Comparisons between the experiment data and modeling results: (a1) and (a2) IL #1; (b1) and (b2) IL-C#2; (c1) and (c2) AB-C

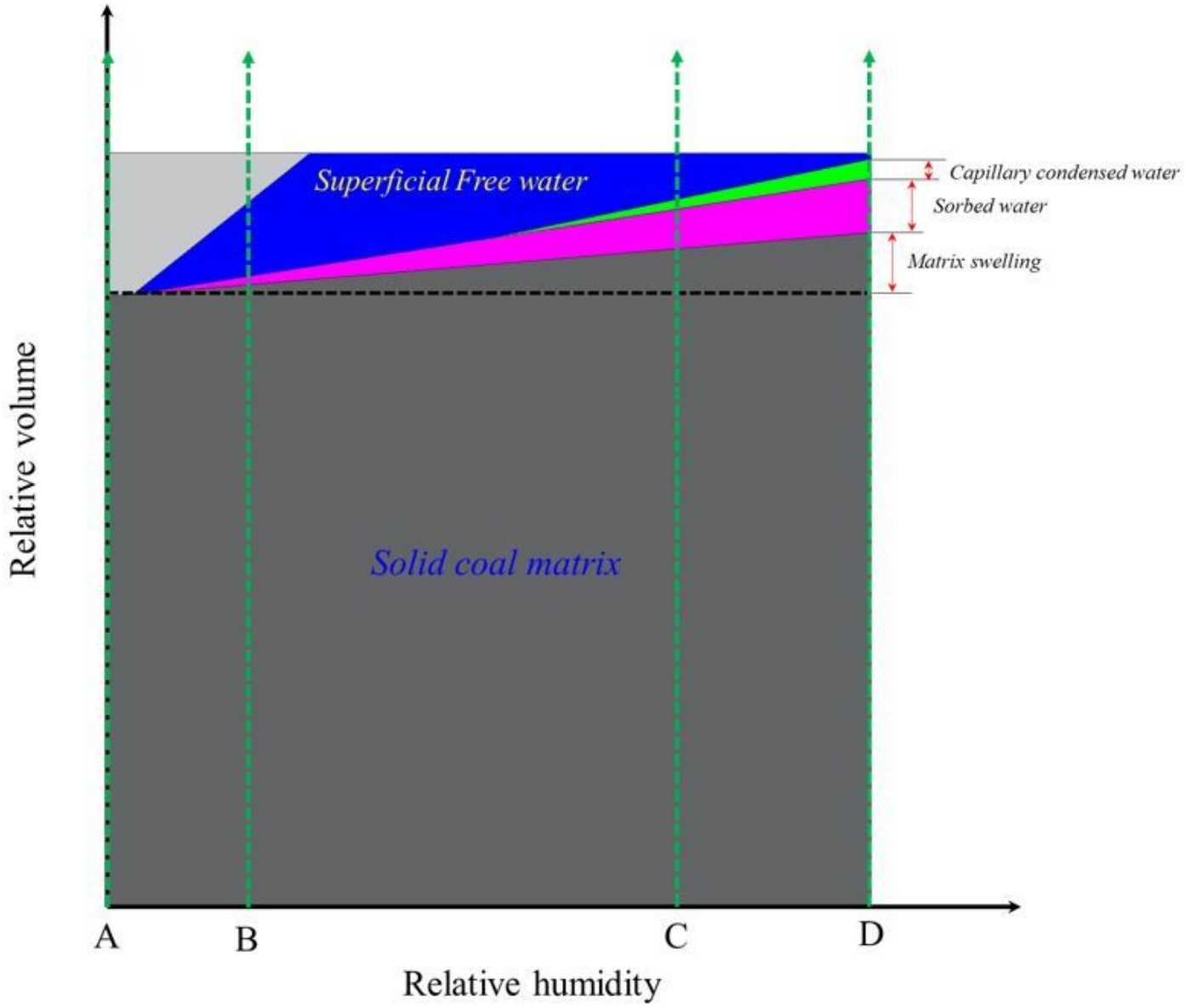

Figure 10

Volumetric phase distribution of solid coal matrix and distinct forms of moisture as a function of relative humidity

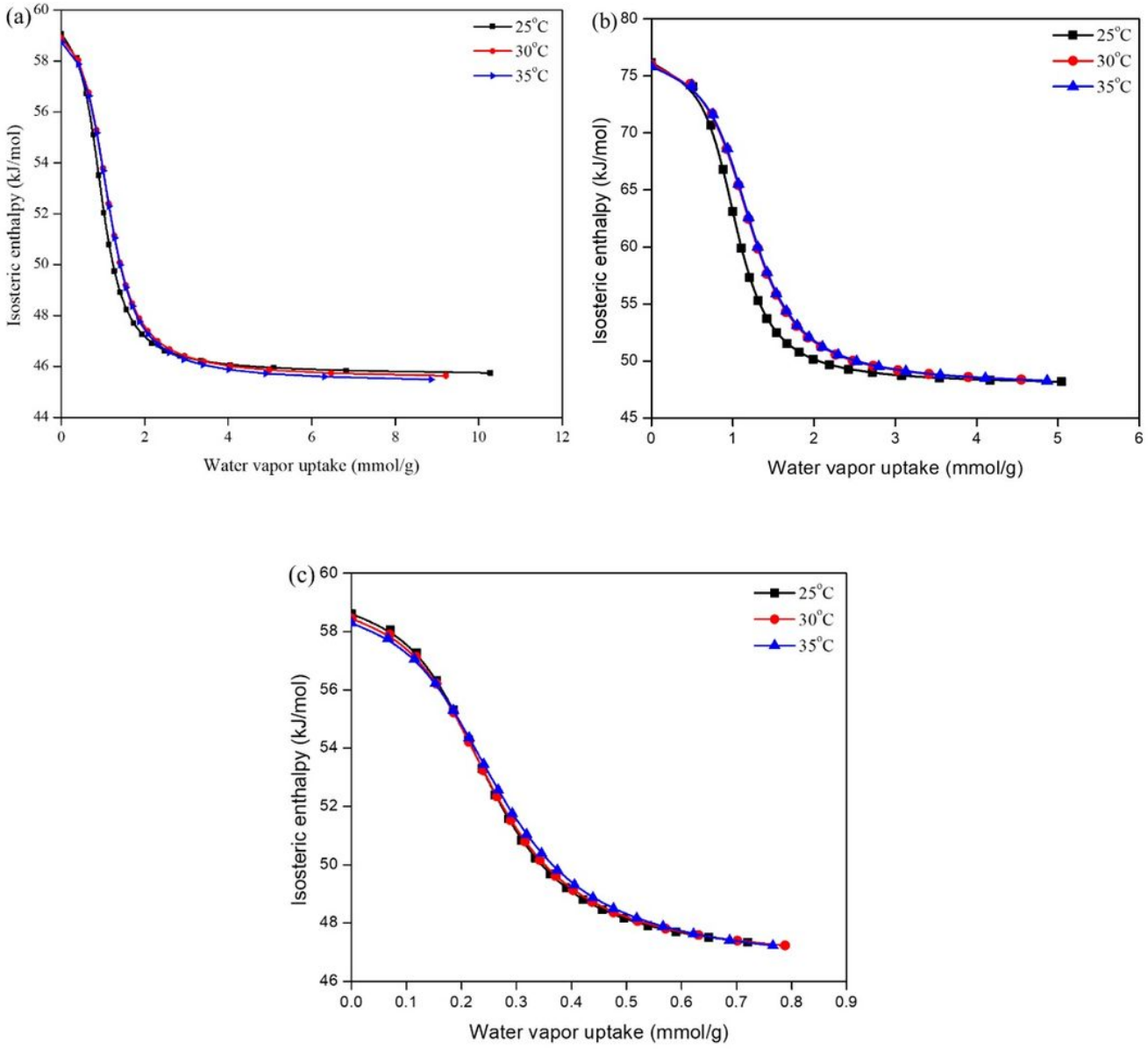

Figure 11

Isosteric heat of adsorption of water vapor in IL-C#1

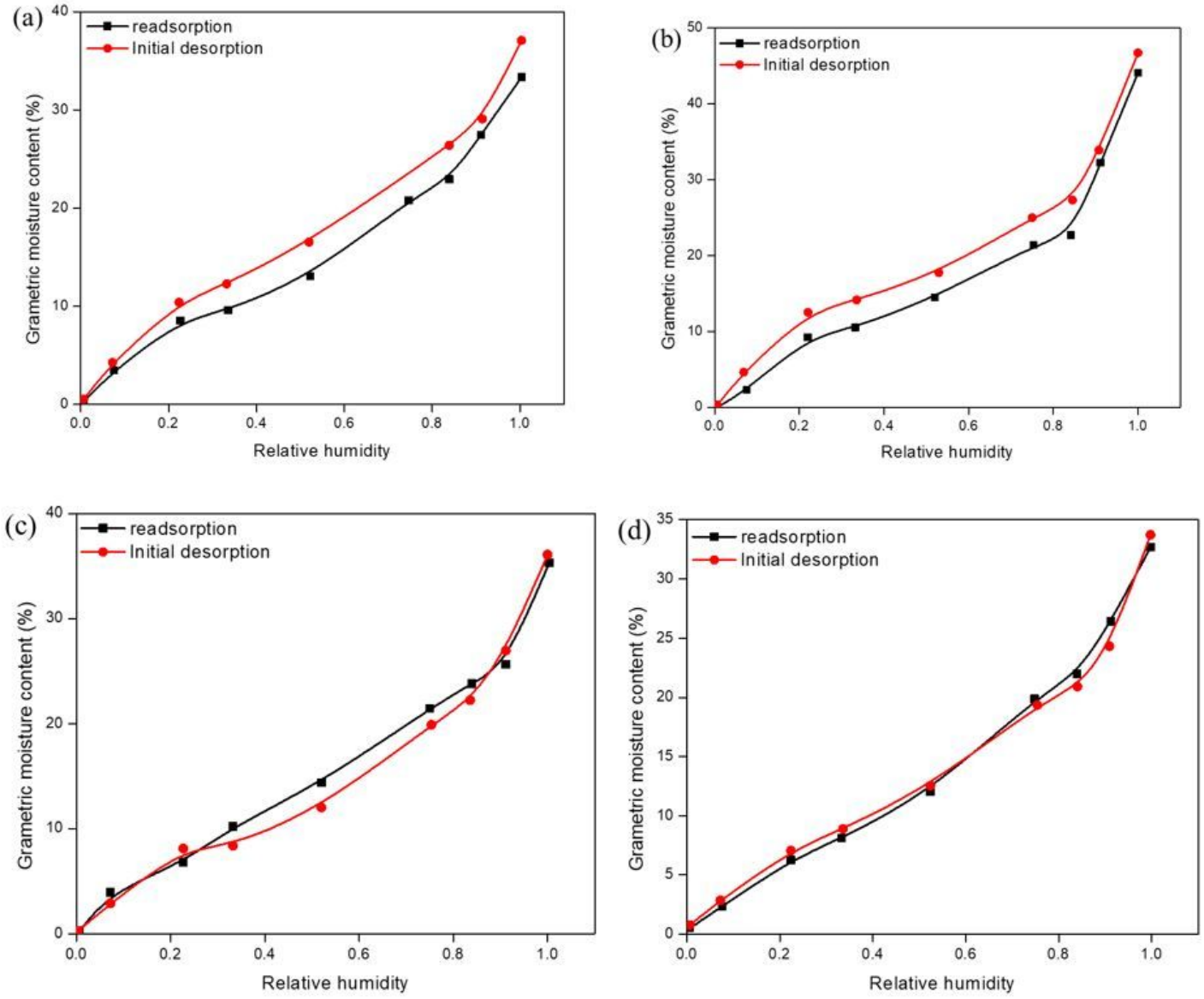

Figure 11

Water desorption-readsorption isotherms of North Dakota lignites as a function of relative humidity [69]. (a) Freedom sample. (b) Gascoyne sample. (c) Glenn Harold sample. (d) Beulah sample.

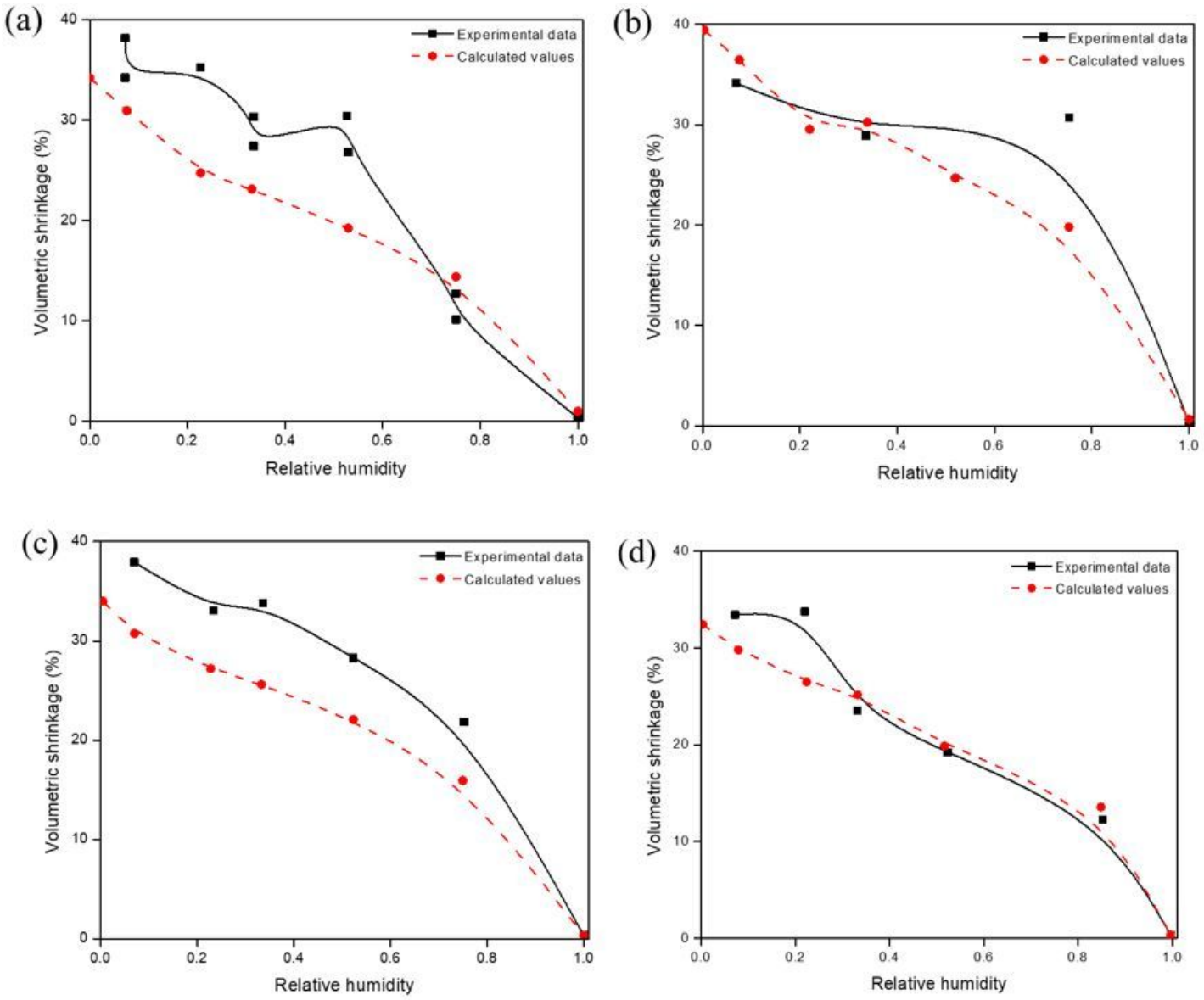

Figure 12

Volumetric shrinkage of North Dakota lignites as a function of relative humidity [69]. (a) Freedom sample. (b) Gascoyne sample. (c) Glenn Harold sample. (d) Beulah sample.